Review Article

Chen Long, Xu Jinghang, Luo Xichun, Liu Zhanqiang*, Wang Bing, Song Qinghua, Cai Yukui, Wan Yi, Gao Xiangyu, and Li Chunlong

Micro/nano manufacturing aircraft surface with anti-icing and deicing performances: An overview

https://doi.org/10.1515/ntrev-2023-0105 received April 10, 2023; accepted July 15, 2023

Abstract: The aircraft surface is prone to icing when flying under windward conditions. It is required to protect the aircraft surface from icing for flight safety. The anti-/deicing performance of aircraft surface is affected by the surface morphology and surface wettability. The hydrophobicity of aircraft surface with anti-/deicing performance is closely related to the surface energy. To satisfy the requirements of anti-/deicing surface processing, the micro/nano manufacturing technologies have been developed to fabricate anti-/deicing functional aircraft surfaces. The icing time and deicing efficiency for aircraft surfaces fabricated with micro/nano manufacturing technologies are dozens of times more than those manufactured by conventional anti-/deicing methods. In this study, the recent technologies of micro/nano manufacturing of anti-/deicing functional surfaces are reviewed. First, the extreme conditions during aircraft flight and the huge potential safety hazards of icing are introduced. Then, the principle of aircraft icing and mechanism of both anti-icing and deicing are summarized. Then, the current micro/nano manufacturing technologies for preparing anti-icing and deicing surfaces, including electrochemical, chemical, laser and wire-cut etching chemical, electrochemical, vapor and plasma deposition, and other processing methods are described. By summarizing

the advantages and disadvantages of different preparation methods, guidance is provided for new methods of preparing anti-icing and deicing surfaces, in order to avoid disadvantages and promote advantages. Fabrication and characterization of nanocomposite materials and composite coatings/thin films with anti-icing and deicing properties are discussed. Finally, the development trend and application prospect of micro/nano manufacturing in the field of anti-icing and deicing are presented.

Keywords: micro/nano manufacturing, aircraft surface, surface engineering, superhydrophobic, anti-/deicing

1 Introduction

The aircraft surface condenses to form ice when the aircraft passes through clouds containing supercooled water droplets and other extreme environments (as shown in Figure 1). Icing causes serious harm to aircraft flying at subsonic speed under visible humidity and temperature close to or below freezing point [1]. There are two main weather hazards according to the safety information announcement (No. 2015-13) issued by the European Aviation Safety Agency. One is the adverse convective weather. Another is the largescale areas with concentrated severe weather, e.g., the Inter-Tropical Convergence Zone [2]. The aircraft flight altitude is ordinarily more than 22,000 feet. The temperature is about -40 to -50°C at which the drizzle forms large-area ice crystals. The aircraft will encounter updraft or downdraft of more than 3,000 feet per minute in some severe convective weather conditions. The severe convective storms are relatively frequent, and the icing as well as ice crystals caused by these storms will greatly affect flight safety [3]. It will have serious impacts on the engine [4], pitot tube probe [5], and other important aircraft components without technical measures to prevent and remove the ice crystals produced. An F-28 flight of Ontario Airlines crashed only 49 s after taking off in 1989. The aircraft stalled and 24 people died due to wing icing. In another instance, the Air France Flight 447 failed to detect the airspeed, and resulted in the shutdown of autopilot

Chen Long: Key Laboratory of High Efficiency and Clean Mechanical Manufacture of MOE, Shandong University, Jinan, China; School of Mechanical Engineering, Shandong University, Jinan, China; Key Laboratory of Icing and Anti/Deicing, China Aerodynamics Research and Development Center, Mianyang, China

Xu Jinghang, Wang Bing, Song Qinghua, Cai Yukui, Wan Yi, Gao Xiangyu, Li Chunlong: Key Laboratory of High Efficiency and Clean Mechanical Manufacture of MOE, Shandong University, Jinan, China; School of Mechanical Engineering, Shandong University, Jinan, China Luo Xichun: Centre for Precision Manufacturing, DMEM, University of Strathclyde, Glasgow, United Kingdom

^{*} Corresponding author: Liu Zhanqiang, Key Laboratory of High Efficiency and Clean Mechanical Manufacture of MOE, Shandong University, Jinan, China; School of Mechanical Engineering, Shandong University, Jinan, China, e-mail: melius@sdu.edu.cn

2 — Chen Long et al. DE GRUYTER

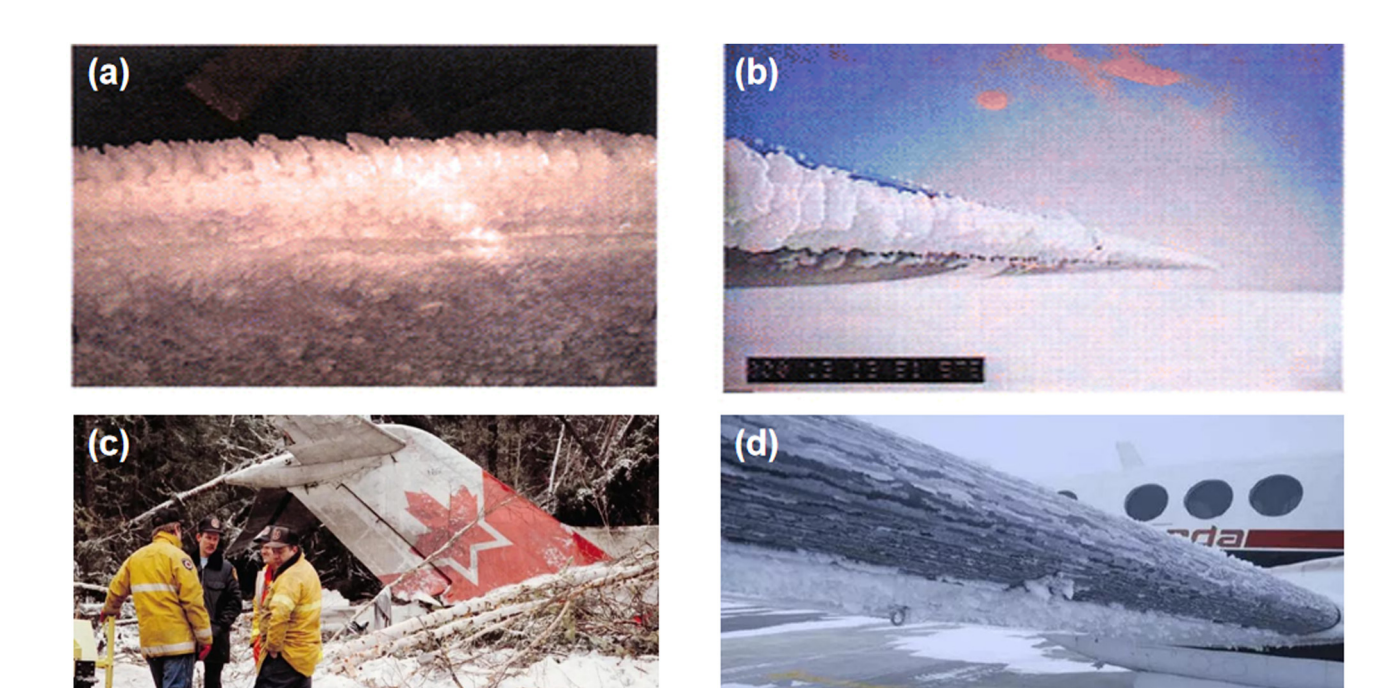


Figure 1: Aircraft surface icing and hazards [1]. (a) and (b) Images of aircraft freezing during extreme weather conditions, (c) aircraft crashing due to icing and (d) aircraft waiting to be cleared of icing.

in 2005. All 228 people on board the plane were killed due to the icing of pitot tube which is the most serious air crash since the founding of Air France.

For the spray anti-/deicing method, the aircraft deicing fluid is composed of isopropanol and propylene glycol, which is safe and pollution-free. However, for a large aircraft, a single spray cost is 30,000–50,000 US dollars, and if the flight does not take off within an hour, it needs to be resprayed. The extremely high cost has sparked exploration for other methods, and choosing anti-/deicing surfaces is a more economical option that can also save maintenance time.

The anti-/deicing technologies have been systematically summarized. Wang *et al.* [6] reviewed the bio-inspired anti-icing strategies such as the surface texture of superhydrophobic (SH) surfaces. The fragile structure of micro/nano surface is one of the key challenges restricting the preparation of SH surfaces. Furthermore, the modifications of the surface and interface materials will improve the stability and robustness of anti-icing technology. Zuo *et al.* [7] analyzed the advantages and disadvantages of the anti-icing and deicing technologies in wind power blades. The combined anti-/deicing technology of ultrasonic and hydrophobic coating is economical and reliable, the technology will be applied in the field of wind power blades. Kreder *et al.* [8] analyzed the application of anti-/deicing under different conditions from the perspective of SH surface

roughness. The SH anti-icing is the research topic of new engineering materials. The basic principles of SH and potential applications of SH surface preparation are reviewed and discussed by Manoharan *et al.* [9]. New prospects are put forward for the future development of SH surfaces, such as the combination of self-cleaning characteristics with other functions, wear resistance, and corrosion prevention.

Generally, the SH performance can be analyzed by measuring contact angles and other parameters of distilled water droplets on the prepared surface. However, for evaluating the performance of anti-icing and deicing surfaces under actual conditions, testing is often conducted in icing wind tunnels to simulate the icing conditions in the atmosphere during real aircraft flight. At the same time, the presence of heating can be controlled to demonstrate the anti-icing effect without heating and the deicing effect during heating [10].

The SH surfaces are beginning to be applied in the field of anti-icing and deicing, and new composite materials are developed. However, there are few summaries and prospects in the field of anti-/deicing surface fabrication with micro/nano manufacturing technology. The micro/nano manufacturing technology is characterized with universality, high precision, and high controllability of processing materials. It is expected to become a new method to enhance the stability and robustness of anti-/deicing surface. As shown in Figure 2,

this review will mainly investigate the latest research progress on the preparation of anti-icing and deicing surfaces by current micro/nano manufacturing technologies. The various micro/nano processing technical conditions, preparation processes, and anti-icing and de-icing effects are summarized in detail. The future developments of micro/nano manufacturing in the field of anti-/deicing are prospected.

2 Principles of anti-icing and deicing

The ice is formatted by phase change process from liquid water or water vapor to solid phase. It starts from the formation of ice core and proceeds with the growth of stable ice core until it is completely frozen. As shown in Figure 3, a stable ice core is generated when the molecular cluster or crystal embryo cluster exceeds the critical size. The ice core continues to grow and form ice crystals [11]. The process of ice core growth is controlled by the heat transfer at the ice water interface and attached to the ice surface by additional molecules. The prerequisite for ice formation is the driving force of solidification, known as supersaturation. There is an energy barrier for transforming high entropy disordered water molecules into

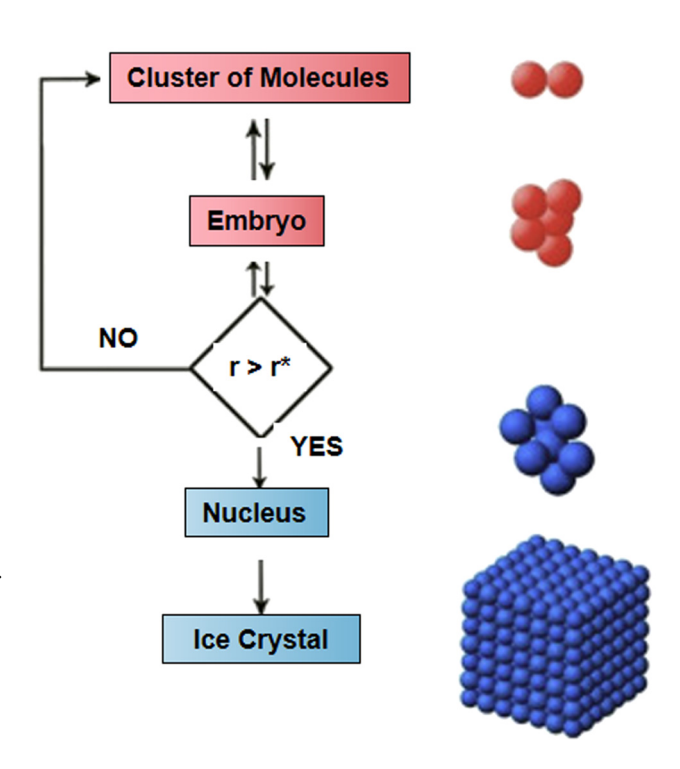


Figure 3: Ice crystal formation process [11].

low entropy highly ordered molecules (ice) according to the second law of thermodynamics. The supersaturation or under-cooling is used as the driving force to overcome

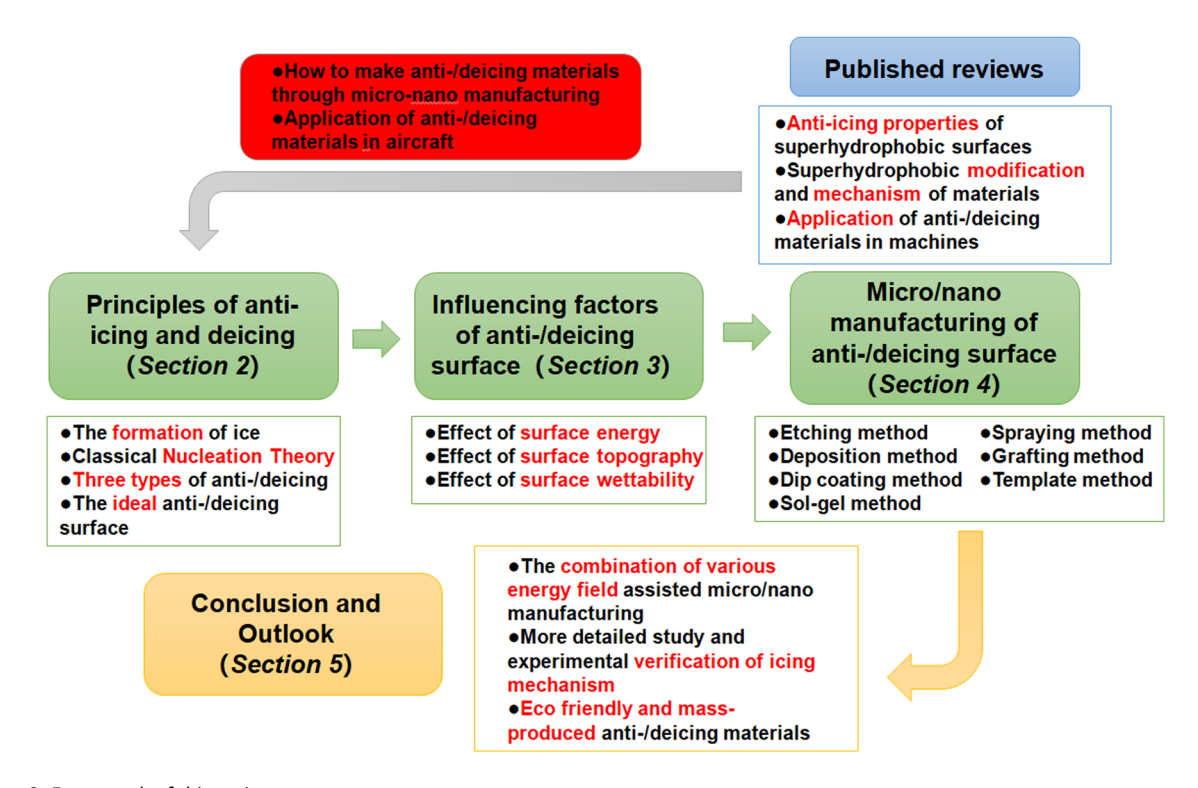


Figure 2: Framework of this review.

the barrier. The unstable crystal embryo is larger than the critical size to form a stable ice core and grows spontaneously to form ice crystals.

The formation of new solid phase requires the generation of crystal embryo clusters with specific size (critical size) based on the carbon nanotube (CNT). This formation process is mainly suitable for low or medium supersaturation [12,13]. Atomic nucleation theory is applied in the case of high level supersaturation [14]. In real-life outdoor environments, the pollutants in the air and precipitation on the outdoor surface of solids play an important role in the nucleation process, which is heterogeneous nucleation. The occurrence of nucleation needs to overcome the Gibbs free energy nucleation barrier, which can be expressed as follows [15,16]:

$$\Delta G = \frac{16\pi \gamma_{\text{IW}}^3}{3\Delta G_{\text{r}}^2} f(m, x),\tag{1}$$

$$m = \cos \theta = \frac{\gamma_{\rm SW} - \gamma_{\rm SI}}{\gamma_{\rm IW}}, \tag{2}$$

$$x = \frac{R}{r_c},\tag{3}$$

$$r_{\rm c} = \frac{2\gamma_{\rm IW}\nu}{\Delta G_{\rm v}},\tag{4}$$

where, ΔG is the free energy of formation of a critical embryo on the nucleating particle; $\Delta G_{\rm V}$ is the Gibbs free energy change of liquid–solid phase transition per unit volume; f(m,x) is determined by the energy and surface shape of the relevant interface, and its value varies from 0 to 1, where 1 corresponds to the homogeneous nucleation limit (no surface involved) and 0 corresponds to ice nucleation without supercooling. m depends on the surface energy of the contact interface. $\gamma_{\rm IW}$ is the ice water interfacial tension, and denotes the surface energy of the solid water interface. represents the surface energy of the solid ice interface. $r_{\rm C}$ is the critical nucleation radius. R is the curvature radius of the surface structure, and x is the surface roughness parameter.

Fletcher [15] deduced the functional formula of f(m, x) for both convex and concave surfaces.

For convex surfaces,

$$f(m,x) = \frac{1}{2} \left[1 + \left(\frac{1 - mx}{g_{v}} \right) + x^{3} \left[2 - 3 \left(\frac{x - m}{g_{v}} \right) + \left(\frac{x - m}{g_{v}} \right)^{3} \right] + 3mx^{2} \left(\frac{x - m}{g_{v}} - 1 \right) \right],$$
(5)

$$g_{y} = (1 + x^2 + 2mx)^{\frac{1}{2}}.$$
 (6)

For concave surfaces,

$$f(m, x) = \frac{1}{2} \left\{ 1 + \left(\frac{1 - mx}{g_c} \right) + x^3 \left[2 - 3 \left(\frac{x - m}{g_c} \right) \right] + \left(\frac{x - m}{g_c} \right)^3 \right] + 3mx^2 \left(\frac{x - m}{g_{vc}} - 1 \right) \right\},$$
(7)

$$g_c = (1 + x^2 + 2mx)^{\frac{1}{2}},$$
 (8)

where g_v and g_c are only used to represent the equations (6) and (8), which are convenient to write and have no practical significance. The equations are only related to m and x. Irajizad et al. [17] plotted the images of f(m, x) on convex and concave surfaces in Figure 4. The ice core formed on the surface is shown in Figure 4(a), where $m = \cos\theta$, θ is different from the contact angle of droplets on the surface. The roughness of convex surface (Figure 4(b)) and concave surface (Figure 4(c)) on the surface is obtained. As x value is less than 1, the nanostructures can affect the f(m, x) function, thus affecting the ice nucleation temperature and ice nucleation rate. However, f(m, x) is the function of m value only when the value of x is greater than 1.

The anti-icing and deicing principles of aircraft surface can be divided into three stages and types based on the icing procedure. In the first two types, the water droplets are prevented from impacting or the vapor condensation is prevented from adhering to the surface and then they are

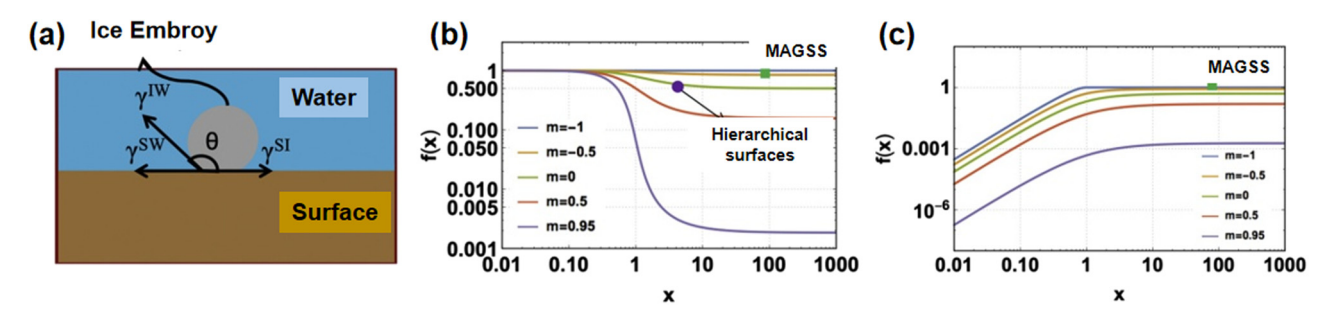


Figure 4: (a) Ice cores formed on the surface and related parameters, (b) images of x and m on the convex surface and (c) images of x and m on the convex surface.

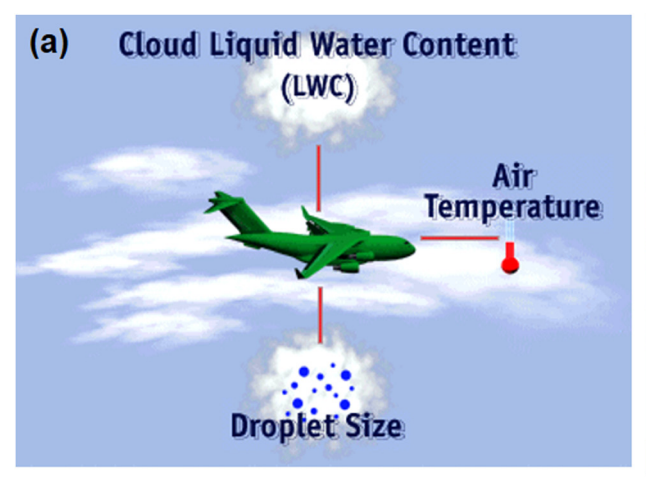
removed from the surface before icing, and the crystallization and nucleation process of water droplets are delayed during freezing process, which is known as anti-icing, this effect is mainly achieved by preparing special microstructures and other methods. In the last type, the adhesion between the ice layer and the surface is reduced after freezing, making it easier for ice to detach from the surface, which is known as deicing.

The specific phenomena are reflected in these three stages with three aspects, respectively. They are the direct roll off of moving water droplets, the self-propelled jumping of condensate droplets, and the sliding off of liquid lubrication layer. The moving water droplets can separate from the surface by bouncing or sliding before freezing when the macroscale water droplets or water flow impact the anti-/ deicing surface. This phenomenon of direct roll off of moving water droplets is due to the anti-/deicing surface having a low contact angle hysteresis (CAH). The direct roll off of moving water droplets is also caused by the liquid droplets when they are in the Cassie state or superlubricity state of easy sliding gas-liquid-solid three-phase contact. Due to the release of surface energy, the self migration small water droplets formed by the condensation of micro water vapor during the fusion process of anti-icing deicing surfaces is called the self ejecting jump phenomenon of condensed water droplets. The sliding phenomenon of liquid lubrication layer causes the liquid droplets to jump off the surface due to the small critical sliding radius on the super lubricated surface [18]. SH surface can inhibit the formation of ice nuclei when the water droplets adhere to the surface. The contact area between the droplets on the SH surface and the base is small, and the possibility of heterogeneous nucleation is slim. The surface has a relatively high ice crystal nucleation potential barrier. In addition, the surface structure

increases the thermal resistance by capturing air or liquid and hinders the transfer of heat between the air and the drops. The formation of ice nuclei is accordingly inhibited, the delayed freezing time is increased and hence the occurrence of icing is delayed [19,20].

As shown in Figure 5, the anti-/deicing surface may lose its anti-icing characteristics in extreme environments. It will result in icing on the surface. Therefore, the anti-/deicing surface should have small adhesion strength of the ice layer. After the surface is frozen, the low adhesion force enables the ice layer formed on the surface to be easily removed under the action of its own gravity, incoming flow, or other external forces [21–23]. Based on the above anti-/deicing principle of aircraft surface, the ice crystal nucleation potential barrier should be increased before icing to prolong the ice crystal nucleation time. At the same time or otherwise, the adhesion strength of the ice layer should be reduced after icing to make the ice layer easier to be removed. Thus, the delayed freezing time and ice adhesion strength can be employed as the criteria to evaluate anti-/deicing performance.

The ideal anti-/deicing surface should have a long delayed freezing time, which makes it hard to freeze when the surface without ice and the small ice adhesion strength makes the ice formed on the surface easy to remove. Delayed freezing time is an important criterion to evaluate the anti-/deicing performance of aircraft surface. The longer delayed freezing time indicates that the surface has a higher ice crystal nucleation barrier, and it is harder to freeze without ice. The delayed freezing time has different definitions based on various experiment setups. It can be defined as the period from the beginning of the droplet cooling on the surface at room temperature when the experiments use fixed droplets [24–29]. It is also defined as the period below the freezing point to the beginning of



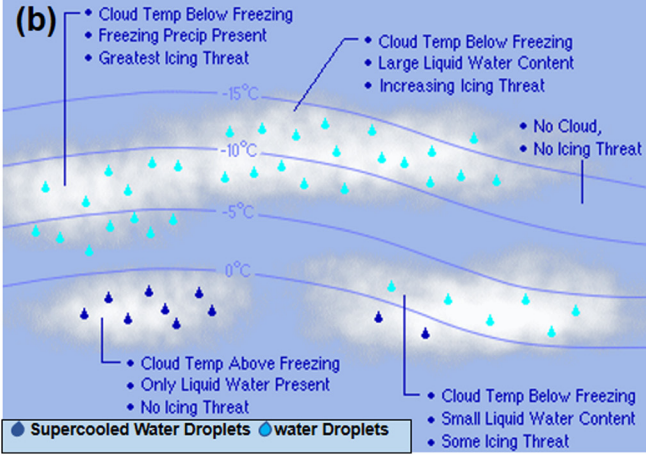


Figure 5: (a) Three influencing factors of aircraft icing and (b) droplets in different airborne environments.

the droplet freezing when it is used in the nucleation and revalorization during the freezing process of fixed droplets [30–33].

When the whole surface is to be observed, the freezing delay time is measured from the beginning of surface cooling, and the propagation process of surface freezing can be continuously observed [34-36]. The freezing delay time of the local observation area is defined as the freezing time from the first droplet to the last droplet [37,38] when observing a small part of the whole surface. Due to the different definitions of delayed freezing time, it is difficult for delayed freezing time to have the property of quantitative measurement of anti-icing and deicing performance for various experimental surfaces. In view of the limitation of delayed freezing time, Kim et al. [39] proposed new definitions of initial ice nucleation time and ice nucleation propagation speed. These definitions can characterize the macro freezing behavior and are used for quantitative analysis of anti-freezing characteristics of bare surface and SH surface.

The adhesion strength of ice layer is another criterion to evaluate the anti-icing and deicing surface performance. The anti-icing surface should have low ice adhesion strength, so that the ice formed on the surface can be easily removed by gravity, natural wind, or other external forces [21-23]. The adhesion force can be divided into tangential stress and normal stress, which refer to as the force required for removing the ice layer along the tangential and normal surface directions, respectively. The factors affecting the adhesion of ice layer include surface contact angle, material deformation, interface morphology, ice crystal structure, temperature, water salinity, etc. [40]. The adhesion strength of ice layer can be measured by centrifuge adhesion test (CAT) [41-44]. The adhesion strength of ice on the surface can be calculated as $F = m_{ice} \times w^2 \times r$, where w is the rotational speed during deicing (rad/s), r is the rotor length, and m_{ice} is the mass of ice. The shear removal stress is calculated by the formula $\tau = F/A$ (where A is the contact area between substrate and ice, and F is the centrifugal shear force). The centrifuge test is hard to get a stress-strain curve.

However, it is still one of the most repeatable ice adhesion tests. It is usually used for the type of impact ice generated by freezing drizzle or in-flight icing simulation [38]. Vertical shear test (VST) is another commonly used method to measure the adhesion strength of ice layer. VST has the advantages of simple equipment and efficiency, but the position of its force probe affects the ice adhesion strength and the stress may be unevenly distributed [40,45]. Rønneberg *et al.* [46] verified the compatibility between VST and CAT.

The properties of ice are highly dependent on the environment and formation conditions, such as temperature, cooling rate, grain size, and crystallization process. Therefore, the formation method of ice determines the nature of ice. Rønneberg et al. [47] verified that the ice type has a direct impact on the ice adhesion strength on the same type of surface. Three ice types were inspected by centrifugal test method. It was measured that the ice formed by frozen drizzle had higher ice adhesion strength than other types of ice did, and the bulk ice had the lowest ice adhesion strength (as shown in Figure 6). The low adhesion surface fabrication is, however, limited by the incompatibility of different ice manufacturing methods and different ice layer adhesion strength measurement methods, because the method for the surface with superior performance of one ice type may not work for the ice type formed in another ice environment. Therefore, the ice adhesion strength should be tested interchangeably for different ice types.

Table 1 shows that the ice formed in various environments have different properties. The properties of ice are highly dependent on environmental and mechanical conditions. The properties of polycrystalline ice are very different from those of single crystal, which depends on the size and orientation of grains. For different types of ice, the same surface will show different anti-/deicing performance. Thus, the ice with different properties should be distinguished according to different generation environments. The multiple tests are necessary to be performed for different icing types when the anti-icing and deicing performance of the surface is tested.

There is an important relationship between aircraft icing and aircraft icing surface morphology fabricated

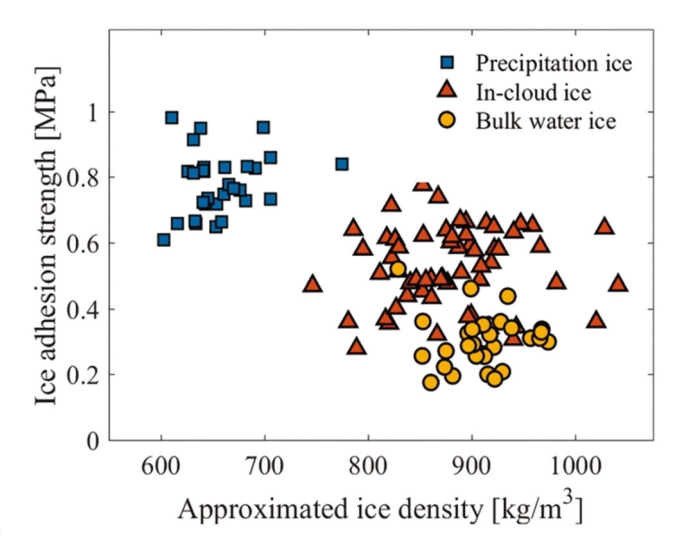


Figure 6: Ice adhesion of different ice patterns [47].

Table 1: Main types of icing

Types of ice	Definition	Ice density	Adhesion
Glaze	A uniform and transparent ice deposit formed by supercooled raindrops freezing on the surface with a surface temperature slightly higher than 0°C or non-supercooled raindrops freezing on the surface with a temperature far lower than 0°C [48]	≥0.9 g/cm ³	+ + + + + + + + + + + + + + + + + + +
Hard rime	An ice deposit composed of particles, containing air inside, formed by supercooled and tiny droplets [48]	0.6–0.9 g/cm ³	+ + +
Soft rime		0.3-0.6 g/cm ³	Strong +
Frost	It has sparse dendrite structure; nucleation from the gas phase by re-sublimation or freezing after condensation [49]	0.05-0.3 g/cm ³	Weak
Snow	A mixture of ice and water. When the air temperature is below -1 or -2 °C, the snow is "dry," but at a temperature close to the freezing point, a thin layer of water covers the ice, forming a characteristic wet ice between ice and water [49]	_	Relatively weak
			Relatively weak

with manufactured technologies. The research status of surface micro/nano manufacturing technologies of aircraft flight icing is required to be reviewed. First, the influence mechanism and research status of aircraft icing surface energy are discussed. Second, the principle and method of micro/nano manufacturing and the research on aircraft anti-icing and deicing are summarized. Finally, the research direction and development trend of micro/nano manufacturing in the field of aircraft surface anti-icing and deicing are prospected.

3 Factors influencing anti-/deicing surface

3.1 Surface energy on anti-/deicing

The anti-/deicing surface performance is mainly affected by the surface morphology and surface wettability. Surface morphology includes surface roughness and surface structure shape. The delayed freezing time and ice adhesion strength is related to these characteristics. The abilities to both resist icing before icing and remove ice easily after icing are influenced by surface morphology. The surface wettability is often described by Young's equation. The larger contact angles between the water droplet and the

solid surface will cause the worse wettability and stronger hydrophobicity. The hydrophobicity of solid surface is related to its surface energy. The lower solid surface energy results in larger static contact angle and stronger hydrophobicity. It is noted that the surface morphology and the surface wettability are influenced by each other. It is necessary to apply the interaction to design the anti-/ deicing surface with low surface energy. The typical theoretical models of surface energy description are shown in Table 2.

In Table 2, it can be seen that the Wenzel's model, due to the addition of a roughness factor r, can more accurately describe the relationship between surface tension and contact angle. Especially in this review, most of the preparation methods are achieved by obtaining surface structures with special morphologies, thereby achieving anti-/deicing performance. Cassie's model proposes a broader equation that uses f to describe the solid–liquid surface fraction, while considering the characteristics of solids and liquids, as well as the influence of roughness, to accurately describe the adhesion of droplets on the surface.

3.2 Surface topography on anti-/deicing

The effect of surface roughness on the delayed freezing time can be characterized by the surface roughness with critical nucleation radius. When the surface structure size

8 — Chen Long et al. DE GRUYTER

Table 2: Typical theoretical models of surface energy

Theory	Model	Contents
Young's equation [50]	$\cos\theta_{\rm S} = \frac{(\gamma_{\rm SV} - \gamma_{\rm SL})}{\gamma_{\rm LV}}$	One of the basic equations of interface chemistry reveals the functional relationship between the relevant surface tension and the contact angle when the droplet reaches equilibrium on an ideal smooth surface.
Wenzel's model [51]	$\cos\theta_{\rm r} = \frac{r(\gamma_{\rm SV} - \gamma_{\rm SL})}{\gamma_{\rm LV}} = r \cos\theta_{\rm S}$	Wenzel's equation defines a roughness factor to consider the increase in surface roughness to emphasize the influence of surface chemistry.
Cassie's model [52]	$\cos\theta_{\rm r} = f \cos\theta_{\rm S} + f - 1$	Considering the air bubbles at the solid–liquid interface in practice, Cassie proposed a more widely used Cassie's model and equation, where f is the fraction of liquid contacting the solid surface.

Where y_{SV} , y_{SL} , and y_{LV} refer to the interfacial tension between solid gas, solid liquid, and gas liquid, respectively. θ_s is the contact angle of smooth surface. θ_r is the contact angle of rough surface. r is the roughness factor. f is the area fraction of the liquid contacting the solid surface.

is smaller than the ice crystal nucleation radius, the functional formula f(m, x) is larger and the heterogeneous nucleation barrier is close to the homogeneous one, which significantly increases the delayed freezing time. On the contrary, when the surface structure size is larger than the ice crystal nucleation radius, the heterogeneous nucleation barrier decreases and the delayed freezing time is decreased.

The shape of surface structure also affects the delayed freezing time [28]. The different surface structure shapes will lead to different solid—liquid contact area and heat transfer resistance. The surface structure shape with small solid—liquid contact area, large heat transfer and thermal resistance has a longer delayed freezing time. Shen *et al.* [53] showed that the layered micro/nano SH surface has a longer delayed freezing time than the single-layer micro/nano SH surface. Due to the double-scale effect of layered micro/nano structure, it can induce more cavitation and increase the thermal resistance of liquid-solid heat transfer, which has a longer delayed freezing time.

The ice adhesion strength on the surface is affected by the surface roughness. Under the same wettability conditions, the ice adhesion strength tends to decrease with the decrease in surface roughness value [48]. Both Wenzel state and Cassie state are common wettability states as shown in Figure 7. The surface roughness has different effects on Wenzel and Cassie wettability states. According to the contact angle equation in Table 2, the apparent contact angle in Wenzel state (θ_a) has a cosine linear correlation with surface roughness factor (r). However, the apparent contact angle in Cassie state is related to the proportion of liquid contacting solid surface [54]. According to the formula from a previous study [51], the increase in roughness will not change the surface hydrophilicity in Wenzel state, while the hydrophobic surface can be more hydrophobic, and the hydrophilic surface more hydrophilic. The apparent contact angle is significantly improved in Cassie state, which makes

it easier to achieve SH state. For SH surfaces, the influence of surface structural parameters on the adhesion strength of ice layer cannot be considered alone, and the droplets should be kept in Cassie state as much as possible. Thus, the droplets being in Cassie state is the key to reduce the adhesion strength of ice layer [55].

3.3 Surface wettability on anti-/deicing

The surface wettability is determined by the cohesion between liquid molecules as well as the adhesion generated by the molecular interaction between liquid and solid. It is usually measured by the contact angle. It is shown that the surface wettability plays an important role in the ice deposition mechanism [56]. The hydrophilic surfaces are more likely to freeze than the hydrophobic surfaces. The static contact angle of hydrophilic surface is less than 90° as shown in Figure 8(a). The static contact angle of hydrophobic surface is greater than 90°, and the water droplets

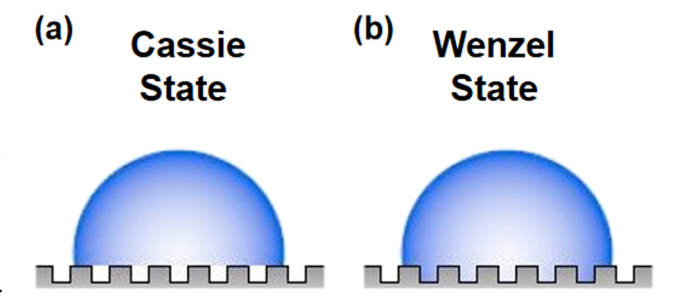


Figure 7: (a) In Cassie state, the liquid and solid are not in complete contact that there is a gas chamber and (b) in the completely wet Wenzel state, the liquid and solid are in close contact, and the interface does not contain gas. The existence of cavitation under the liquid drop in Cassie state leads to a higher backward water contact angle (WCA). In Wenzel state, the increase in solid–liquid interaction area leads to lower WCA and stronger water droplet adhesion [48].



Figure 8: (a) Hydrophilic surface (contact angle θ less than 90°) and (b) SH surface (contact angle θ more than 135° and low CAH) [15].

tend to be bead. For SH surfaces with contact angles greater than 135°, the water droplets are more spherical as shown in Figure 8(b).

The delayed freezing time is also influenced by the surface wettability influence. The low surface wettability can significantly improve the delayed freezing time [20]. The decrease in surface wettability causing the increase in contact angle is due to the reduction in solid—liquid contact area, the delayed heat transfer process, the delayed supercooling droplets, and the prolonged freezing time. In addition, the reduction in solid—liquid contact area reduces the proportion of droplet nucleation rate at the solid—liquid interface in the droplet assembly nucleation rate. The nucleation process is closer to the mean nucleation. The ice crystal nucleation barrier is then improved and the delayed freezing time is increased.

Forward and backward contact angles represent the maximum and minimum possible contact angles for given liquid/solid combination, respectively. They can be measured using the tilt base option or using the addition/removal volume method. In the case of inclined base method, when the solid tilts from 0° to 90°, the uphill angle (or backward angle) decreases, while the downhill angle (or forward angle) increases. The difference between advancing contact angle

and receding contact angle is called CAH. Figure 9(a) shows the static contact angle, and Figure 9(b) shows the movement of droplets on an inclined surface.

The design of ice repellent surface should not only have high static contact angle, but also maintain non wetting SH state and low hysteresis contact angle under the hydrodynamic pressure of impacting droplets [57]. The delay time of the surface with low hysteresis contact angle is longer. The lower CAH reduces the adhesion and dynamic friction between the droplet and the surface, which resulted in a higher possibility of hitting the supercooled droplet escape (*i.e.*, rebound) from the surface.

The effects of surface wettability on the anti-icing and deicing performance of the surface before icing are relatively consistent. However, the effect of surface wettability on the adhesion strength of ice layer is controversial. Some studies [58–60] claimed that the ice adhesion strength decreased with the surface wettability. However, other studies reported that there was no correlation between surface wettability and ice adhesion strength [61]. Although the influence of surface wettability on ice adhesion strength has not been researched clearly, the large surface contact angle and small contact angle lag can reduce the solid–liquid surface contact area. The solid–liquid surface adhesion is then decreased, which is helpful to reduce the ice adhesion strength [62]. Thus, the surfaces with SH properties may have weak ice adhesion [63].

4 Anti-/deicing surface with micro/ nano manufacturing

It can be realized by controlling the surface roughness (physical dominant) and reducing the surface energy (chemical dominant) to obtain SH anti-icing/deicing surface.

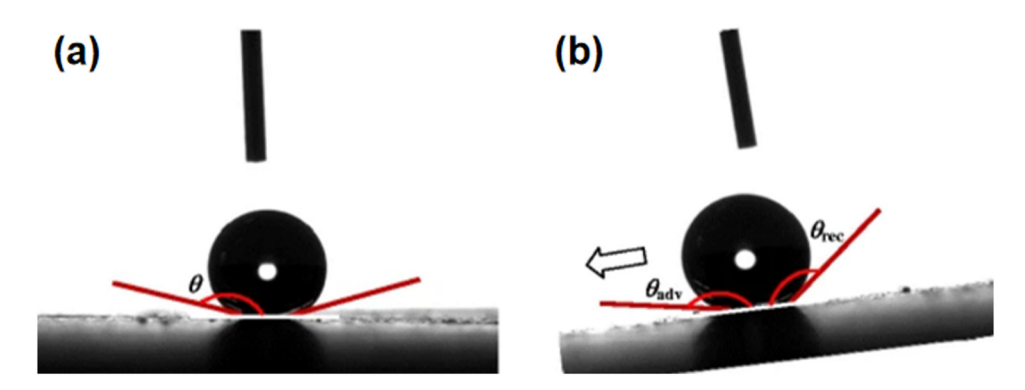


Figure 9: (a) Static contact angle θ , and (b) the movement of a droplet on an inclined surface (θ_{adv} is the forward contact angle, θ_{rec} is the backward contact angle, and the lagging contact angle is the difference between the forward contact angle and the lagging contact angle) [57].

Generally, the material surface is physically or chemically etched as the first step to prepare the rough surface with micro/nano structure, and then the micro/nano structure is chemically modified by low surface energy substances such as silicone to reduce the surface energy. The micro/nano manufacturing methods of SH surfaces mainly include etching [66–80], dipping coating [91–97], spraying coating [98–120], sol–gel [133–136], *etc*.

4.1 Electrochemical, chemical, laser, and wire-cut etching

Etching process is one micro/nano manufacturing method mainly through physical or chemical modification to improve the roughness of the substrate and to obtain low surface energy substances as to obtain super-hydrophobic surface and anti-/deicing performance.

Sun *et al.* [66] etched the Al substrate electrochemically to obtain the hierarchical porous structures which were composed of AloOH and Al_2O_3 . After injecting silicone oil, the obtained slippery liquid infused porous surface (SLIP) presented a water roll-off angle of 3°. The freezing rain experiment was carried out on them. The freezing adhesion of SLIP was reduced from 36.8 to 3.025 N, which was 91.8% lower than that with bare aluminum surface. The SLIP had excellent anti-/deicing performance and corrosion resistance in extreme environments. Song *et al.* [67]

prepared a layer of micro/nano binary rough structure composed of uneven platform structure on the die steel substrate by electrochemical etching (Figure 10). After modified by fluoroalkylsilane (FAS), the WCA of the sample surface was 167.2°, while the water sliding angle (SA) was 4.3°.

Jin et al. [68] fabricated the layered structure on pure aluminum plate by the combination of electrochemical corrosion and hydrothermal treatment (as shown in Figure 11(a)). The hydrothermal growth of nano wool spheres significantly increased the specific surface area, which was conducive to the complete modification of the surface with low free energy materials. Then, the fluorination modification was carried out to obtain SH surface with WCA of 164° and SA of 1.5°. Compared with the prepared micron structure and nanostructure, the ice extension time of micro/nano hierarchical structure was 1,697 s, while the ice extension time of micron structure and nanostructure were 431.2 and 708.3 s, respectively. The ice adhesion strength of the sample was 35.7 kPa. The strength was much lower than that of 720.5 kPa on the untreated surface, which was presented with good anti-icing performance. However, it was shown that the SH anti-/deicing performance fabricated by only electrochemical etching was extremely limited, and the micro/nano structure was required to be further modified. Xu et al. [69] carried out electrochemical machining on the magnesium alloy plates to fabricate the excellent performance by controlling the processing current density and processing time. The fabricated magnesium alloy was immersed in FAS ethanol solution. The super hydrophilic magnesium alloy surface was then successfully transformed

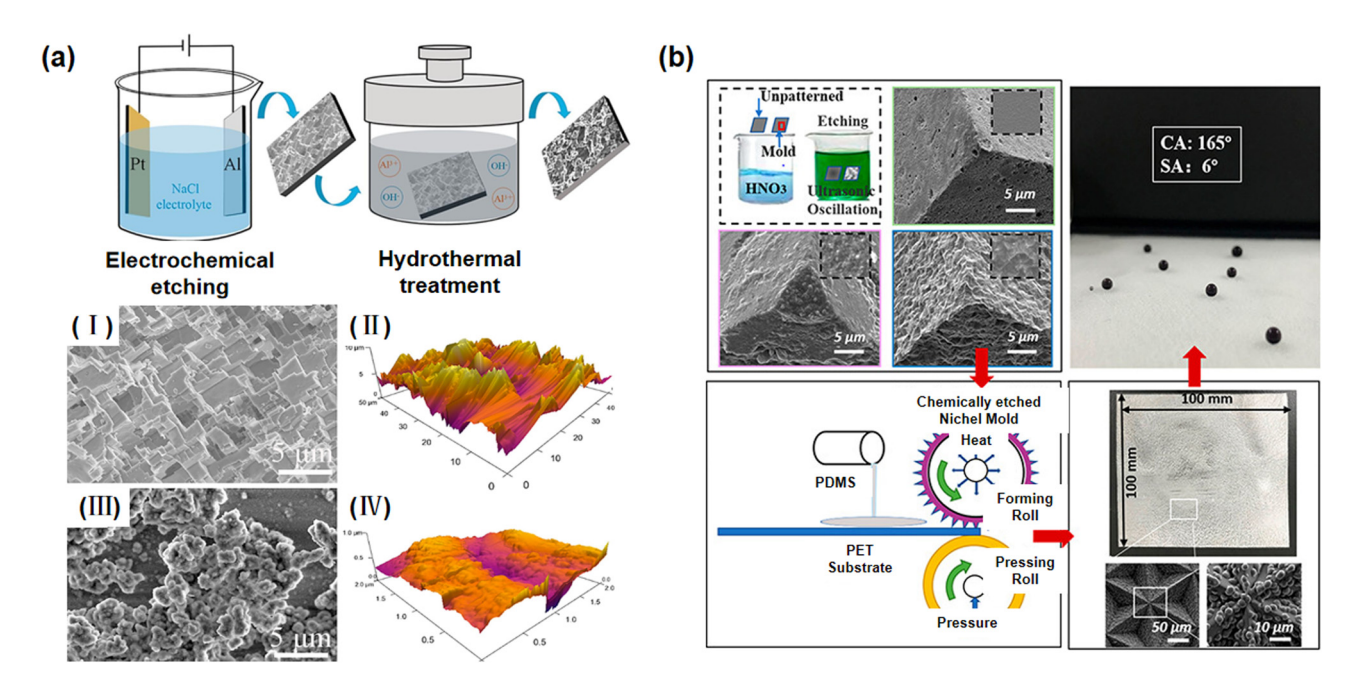


Figure 10: (a) Schematic diagram of etching device (a) (I–II) image after etching of Al substrate, (a) (III–IV) image after FAS processing [67], and (b) Ni substrate [74].

into SH one. The WCA was 165.2° and the water tilt angle was about 2° for the magnesium alloy SH surface. Though the preparation process with electrochemical etching is simple, it can only process and be applied to the conductive materials, and it is hard to process metal materials with weak activity.

The chemical etching process is simple and the product cost is low. The etching liquid is mostly strong corrosive liquid. It has been widely applied in the processing of SH surfaces. Zhang et al. [70] took the concentration of NaAlO₂ and reaction time as factors, prepared the superhydrophobic surface by chemically etching the aluminum substrate, covered with a large number of smaller conical particles, and the micro bone array was formed by highly crystalline Al(OH)₃ on the aluminum sample surface. The adhesion of ice was measured with a dynamometer. The adhesion of the original aluminum plate and the prepared aluminum plate were 168 and 33 kPa, respectively. The prepared SH aluminum plate had better anti-icing adhesion performance. Lu et al. [71] applied the electrochemical etching method to construct coral like micro/nanoscale rough structure on aluminum substrates. After being modified by 1H,1H,2H,2H-perfluorodecyltriethoxysilane, the waterdrop slip probability value reached 96.7% when the inclination angle was within the range of 25~30°. The WCA was about 169°. Barthwal et al. [72] fabricated a rough structure through chemical etching and anodic oxidation, and then used polydimethylsiloxane (PDMS) and injected silicone oil for surface modification to prepare a SH surface. The ice adhesion strength of the modified slippery oilinfused PDMS coating was low, which was 35 \pm 15 kPa. Li et al. [73] etched the surface of magnesium alloy with a mixed solution of NaCl and NaNO3 to manufacture a micro rough structure. After fluorination modification, the SH

magnesium alloy surface with a contact angle of about 162° and the SA of only 3° was fabricated.

Xu et al. [74] prepared nickel templates by HNO₃ chemical etching, and fabricated large-area micro/nano structured PDMS films with SH properties by thermal curing process (Figure 10(b)). First, the different surface morphologies of templates were manufactured by changing the concentration of chemical solution and etching time. Then, the PDMS films with different wettability were prepared, in which the contact angle >160° and SA <10° could be achieved. Finally, the large-area PDMS film was obtained by roll to roll (R2R) thermal curing process. After contact angle of PDMS film is 164.9°, abrasion treatments, the average and the average SA is 6.2°, indicating that it still has SH characteristics. Wenxuan et al. [75] applied the method of ultrasonic chemical etching combing with hydrothermal treatment to manufacture the SH surface. The cleaned aluminum plate in hydrogen fluoride solution was immersed first. Then, it was mixed with acid solution and hot water in turn. Finally, the FAS-17 solution for etching plate was modified. The SH surface with Hydrangea like micro/nano structure was manufactured. It was with the contact angle 161.4° and the SA was less than 1°. Compared with the bare surface, the freezing time of the prepared surface was delayed by about 4~5 times on average.

In recent years, the laser ablation is becoming one faster and less polluting choice, especially for some alloys with strong corrosion resistance in the field of micro/nano manufactured surface with anti-icing and deicing performance. The laser ablation is characterized with high machining precision and simple machining process. It can efficiently construct complex micro/nano rough structures, but it is often expensive. Yang *et al.* [76] employed ultra-short pulse femtosecond laser system to prepare

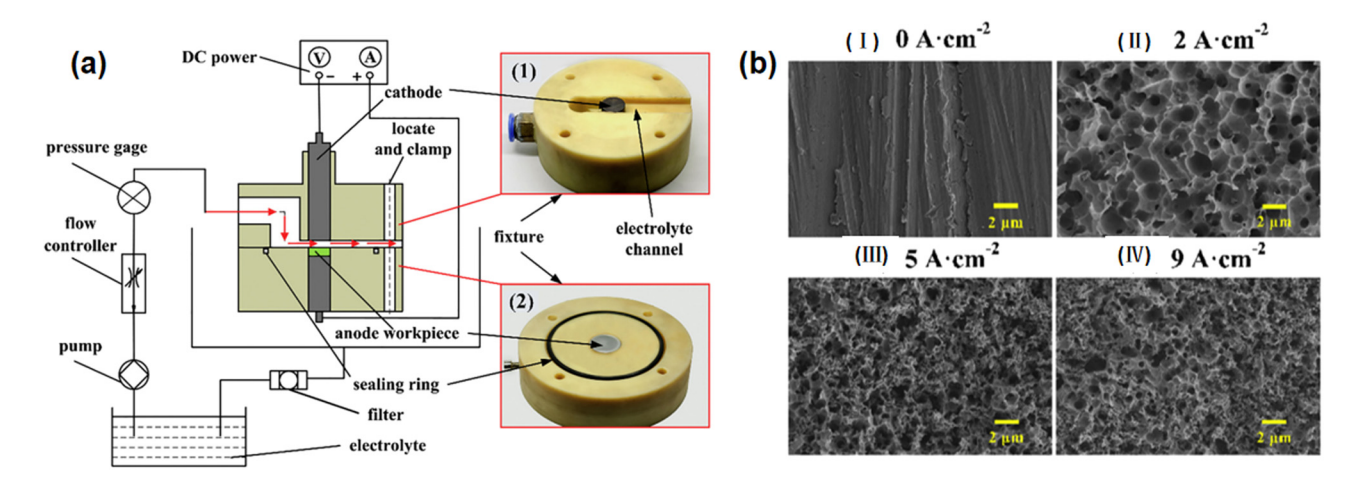


Figure 11: (a) Process equipment, (a) (1) vertical view (a) (2) bottom view and (b) (I–IV) SEM images with different intensities [66].

TC4 alloy surface with a spacing of 50 µm trench microstructure (Figure 12). The groove depth of TC4 alloy surface increased with the laser scanning speed. The contact angle first increased and then decreased with the increase in micro/nano structure size. When the scanning speed was 2,000 mm/s, the maximum contact angle was 103.26°, and the maximum droplet freezing time was 60 s. Liu et al. [77] fabricated the micro/nano surface on TC4 substrate by laser ablation technology. The TiO₂ nanostructure was formatted by hydrothermal treatment. The sample was modified with the FAS-17 solution at room temperature and fully dried to obtain the sample (Figure 10(b)). The freezing time was delayed from 34 min to more than 90 min relative to the control sample whose surface was treated only by the laser processing. The high precision of laser ablation compared with other etching methods enables it to prepare more precise and regular periodic texture patterns. The high precision of laser ablation compared with other etching methods enables it to prepare more precise and regular periodic texture patterns. Milles et al. [78] used direct laser interference patterning, direct laser writing, and combination methods to prepare five different periodic texture patterns on the aluminum cantilever. All structures show superhydrophobic performance, with static contact angle exceeding 166° and SA below 10°. Different textures have

different performance for specific icing conditions, and surface patterns with larger feature sizes often have higher interfacial shear stress.

Gaddam et al. [79] reported that two-tier multiscale (MS) nanofibers had the best anti-icing performance compared with the laser induced single-tier nanofibers on the stainless steel substrate. Within 5 min after the beginning of the freezing process, the surface of LIPS was covered by frost. For the surface with double-layer MS structure, there was only 60% of the MS surface area was covered by frost after 50 min, which indicated that the anti-icing performance was significantly improved. In addition, the double-layer MS had excellent wear resistance and maintained good anti-/deicing performance even if the surface encountered severely repeated wear. Hou et al. [80] etched micro column arrays with different distances between columns on the surface of Si substrate by plasma etching, and the SH surface was obtained after modification. The icing delay time can reach 1,295 s when the distance between columns was 70 µm. When the distance between columns is 30 µm, the deicing effect on the surface was the best, and the ice adhesion strength was 16 kPa.

Moreover, the electrochemical surface processing can increase the service life of composite materials to a certain extent, and can ensure the relative integrity of surface

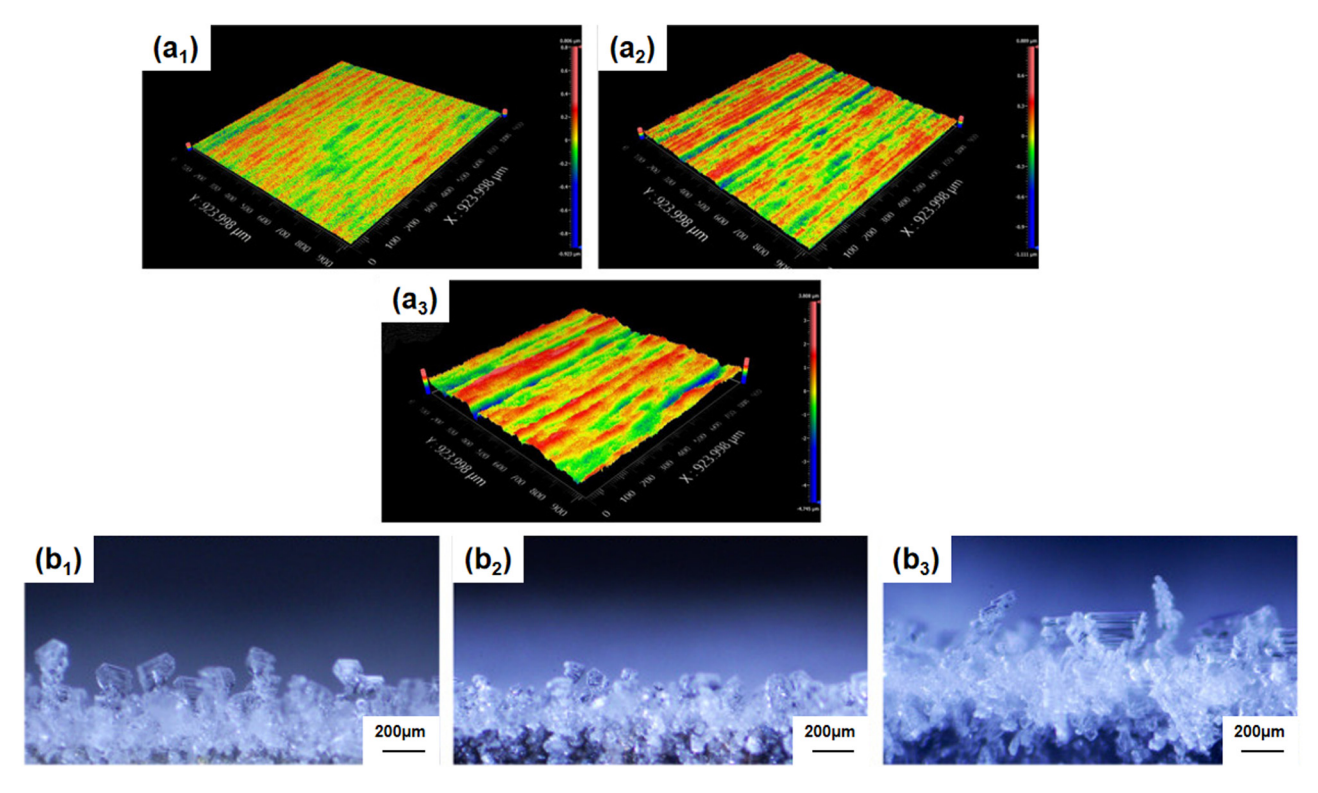


Figure 12: (a) White light interference microscope image of TC4 alloy surface at different scanning speeds: (a₁) V = 5,000 mm/s; (a₂) V = 2,000 mm/s; (a₃) V = 400 mm/s, and (b) (b₁-b₃) surface frost crystal morphology at different scanning speeds [76].

microstructure after long-term use. Femtosecond laser-induced methods also have an impact on the service life of the surface. Compared to untreated surfaces, the wear resistance of electrochemical treated surfaces has also been improved, and their anti-icing performance can still be maintained after multiple wear cycles [79].

The etching method can fabricate the SH surface on the substrate interface with good stability and durability, but it often needs other low surface energy materials for modification. The processing takes a long time, and the mechanical properties of the etched surface are affected to some extent. There are high requirements for the substrate material.

4.2 Chemical, electrochemical, vapor, and plasma deposition

The deposition is a micro/nano manufacturing method in which the deposition agent matrix is pre- prepared in the deposition solution, or the film with special micro/nano structure is formed on the substrate through atomic and intermolecular chemical reaction through gas transfer reactants. The super hydrophobic micro/nano structure can be fabricated by deposition method to realize the anti-icing and deicing performance.

Chemical deposition and electrochemical deposition are the two most widely applied manufacturing methods. Huang et al. [81] deposited a spherical structure with a diameter of hundreds of nanometers in the mixed solution of nickel sulfate and potassium persulfate on the stainless steel substrate. After being modified by perfluorooctanoic acid, the surface of SH stainless steel sheet with a contact angle of about 158° was obtained. Jia et al. [82] soaked the magnesium alloy sheet in silver nitrate solution and prepared a SH membrane with network and uniform microsphere structure composed of irregularly arranged nanostructures on the surface (Figure 13(a)). The surface of the treated magnesium alloy has high hydrophobicity characteristics with the WCA of 153° and water SA of 4°. Zhu et al. [83] soaked the Cu sheet in silver nitrate solution to deposit coral like rough structure on the surface of the copper sheet. After being modified with perfluorooctanoic acid, the SH copper surface with a contact angle of about 163° was fabricated. The chemical deposition method can replace the products with less active metals (e.g., expensive nickel and silver).

The electrochemical deposition method has lower manufacturing cost, more stable structure and improved wear resistance. Xiang *et al.* [84] deposited Ni on the low carbon steel substrate and then deposited Cr coating on the Ni (Figure 13(b)). The maximum WCA of the coating modified by myristic acid was $167.9 \pm 2.4^{\circ}$, and it still maintained good

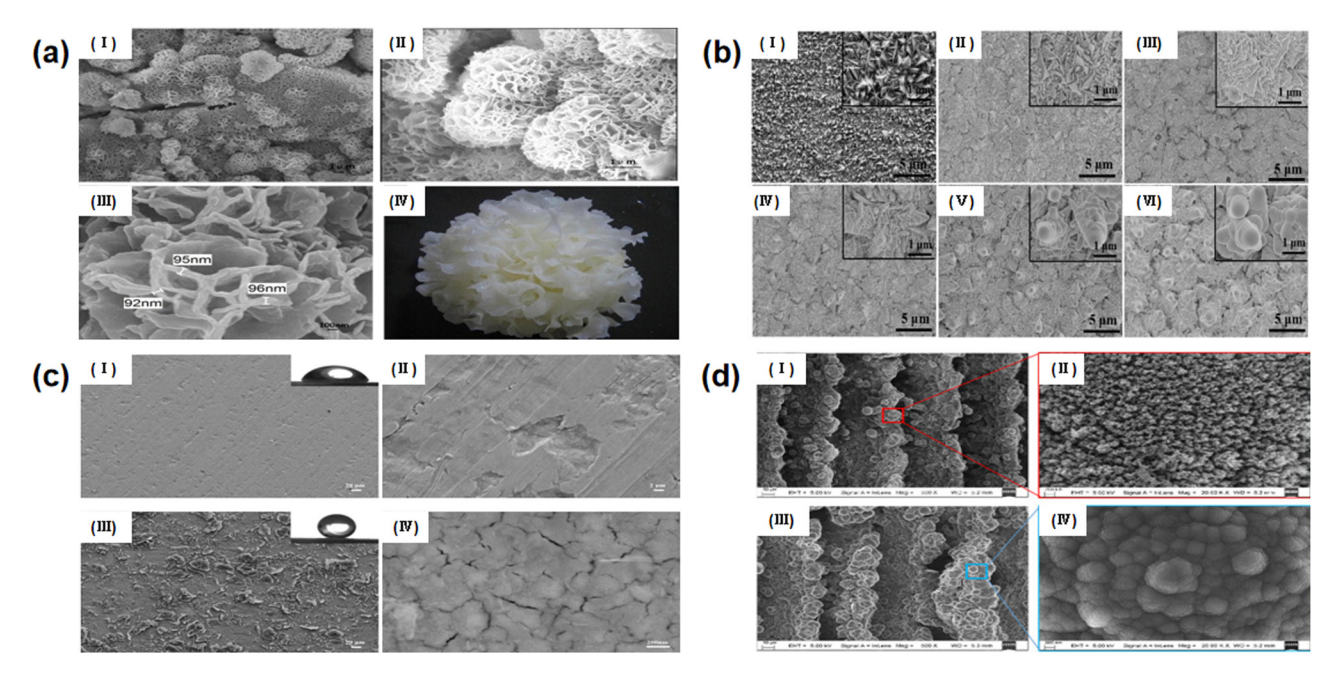


Figure 13: (a) (I-IV) SEM images of chemically deposited surfaces at different magnifications [82], (b) (I-IV) SEM images of surfaces after 0-120s of Cr deposition [84], (c) (I-II) SEM images of untreated surfaces, (c) (III-IV) SEM images of electrochemical deposition [85], (d) (I-II) TEM images of plasma deposition of Cr, and (d) (III-IV) TEM images of plasma deposition of chromium carbide [89].

hydrophobicity after 100 abrasion cycles. Tan et al. [85] deposited micro/nano rough structure dominated by micro/nano laminated crystals on the surface of iron sheet by electrochemical deposition method (Figure 13(c)). After modification with stearic acid, the SH surface with contact angle of about 154° and SA of about 2° was fabricated. The SH surface had good anti-corrosion performance. Liu et al. [86] used the ethanol mixed solution of cerium nitrate hexahydrate and myristic acid as the sedimentation solution to deposit the coral like rough structure on the magnesium alloy substrate. Due to the low surface energy characteristics of myristic acid, the surface of SH magnesium alloy sheet with a contact angle of about 160° was obtained. Su and Yao [87] deposited Ni nanoparticles (NPs) on the Cu surface by electrochemical deposition method. After being modified by 1H,1H,2H,2H-perfluorodecyltriethoxysilane, the surface of pineal layered micro/nano structure and low surface energy fluorinated components was manufactured. The SH Cu surface with contact angle of 162° and SA of about 3° was obtained.

The general deposition method usually consumes a long time. The efficiency can be greatly improved by using the vapor deposition method, plasma deposition method, and the coating thickness and uniformity can be guaranteed easily. Deng et al. [88] deposited a silica shell on the soot layer using chemical vapor deposition (CVD) and coated the hydrophilic silica shell with hemifluorosilane. The super hydrophobic coating, which was easy to manufacture, is transparent, and can rebound oil, was prepared. The WCA of the coating was 165 ± 1°, and the SA was less than 1°. Liu et al. [89] prepared parallel microstructure on stainless steel substrate sample by laser ablation, and then the sample was inserted into the vacuum chamber for sequential plasma deposition of Cr/chromium carbide/diamond-like carbon (DLC)/F-doped diamond-like carbon (F-DLC) to prepare SH coating (Figure 13(d)). The content of F element in the coating was 34.6%, which can significantly reduce the surface energy of F-DLC coating and improve its hydrophobicity. The supercooled water droplets are easy to roll off the coating surface with a WCA of 152° and a water SA of about 8°, which presented that the coating had good anti-icing ability. Niu et al. [90] took the advantage of the layer-by-layer (LbL) assembly technique that was compatible with different substrates, the positively charged poly(diallyldimethylammonium)/MXene) $_n$ multilayers with varied numbers of deposited bilayers (n) can be fabricated on different substrates. Its photothermal effect can be effectively employed in anti-/deicing field.

The deposition method has the characteristics of wide processing ranges and simple preparation process. It can process the complex surfaces. However, the SH surface prepared by the electrochemical deposition method is apt to wear and has poor mechanical strength, which makes it hard to meet the performance requirements under harsh conditions. The SH surface performance fabricated by deposition method needs to be strengthened through repeated depositions and additional manufacturing processes.

4.3 Dip coating

The whole coated objects are immersed in the tank containing the coating. These objects are then taken out of the tank after a short time, and the excess coating liquid flows back into the tank. This manufacturing technique is called dip coating method. The treated substrate is immersed in low surface energy material to obtain low surface energy coating. The dip coating thickness fabricated by this micro/nano manufacturing method can be controlled in the range of $20{\sim}30~\mu m$.

As shown in Figure 14, Lo et al. [91] chemically etched the Al substrate in HCl solution to obtain graded micro/ nanostructures, and then the sample was immersed in toluene solution with different FD-TMS/PDMS-TES weight ratio to obtain the coating. The WCA of the coating was about 165°. The surface presented relatively low ice adhesion strength of 25.3 kPa when the PDMS was 2.9 wt%, and the strength was only 47.2 kPa in 100 freezing/melting cycles, which showed excellent durability and anti-/deicing performance. Peng et al. [92] dispersed NH₄HCO₃ powder in the mixed solution of poly(vinylidene fluoride) (PVDF) with N,N-dimethylformamide and coated it on wind turbine blades. The WCA and SA of SH PVDF coating were 156 ± 1.9° and 2°, respectively (Figure 14(b)). Tan et al. [93] fabricated PVDF/SiO₂ coating by dip coating method as shown in Figure 14(c). The WCA was 159°, and the SA was less than 3°, which presented superhydrophobicity and remarkable anti-/deicing performance. The coating can reduce the adhesion of ice layer on the substrate by 40%. Yang et al. [94] manufactured SiO₂/ poly (vinylalcoho1) (PVA)/ polyacrylic acid (PAA)/fluoropolymer hybrid SH coating with biomimetic peg function on wood samples by dip coating method (Figure 15(d)). The fabricated bionic wood was characterized not only with superhydrophobicity (the WCA was 159°) but also with excellent stability and water resistance.

Cohen *et al.* [95] synthesized SiO₂ NPs with SH coating with better durability by dip coating method. The contact angle of fabricated SH surface was more than 155° and the SA was less than 5°. The ice wind tunnel experiment showed that the SH coating could reduce the ice adhesion and achieve the effect of anti-/deicing. Gwak *et al.* [96]

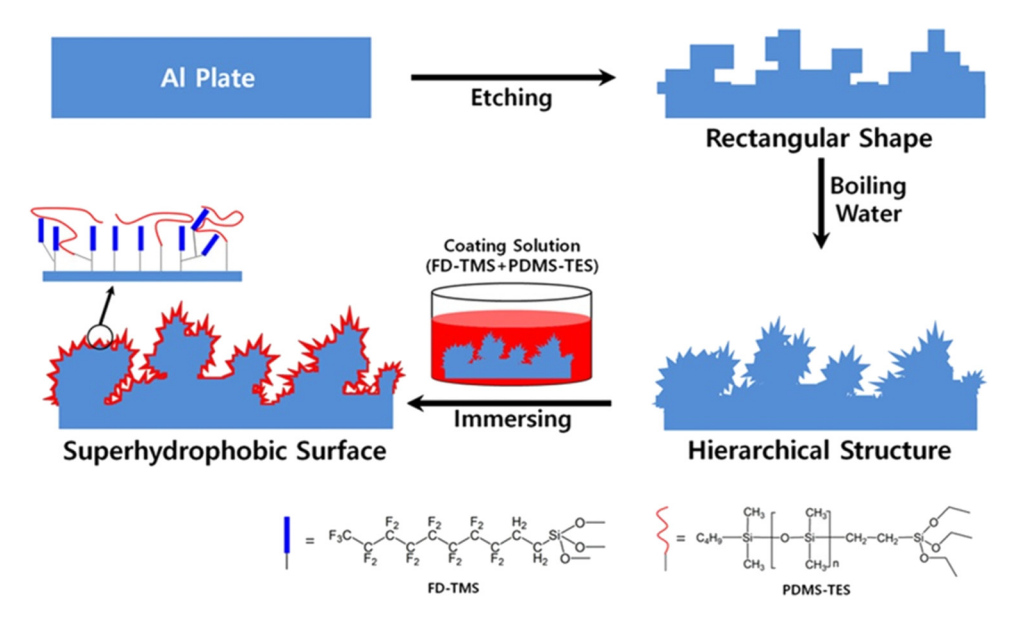


Figure 14: Manufacturing process by dip coating method [91].

coated Al substrate with antifreeze proteins (AFPs) from the Chaetoceros neogracile (Cn-AFP). The Al was fused with Cn-AFP to make Cn-AFP wrap Al. Compared with bare Al substrate and traditional hydrophilic Al coating, the AFPs significantly hindered the freezing of aluminum surface. This effect was due to the high thermal hysteresis value of Cn-AFP and its ability to reduce the freezing point. Zhang *et al.* [97] fixed the reinforced coating through the adhesive

expansion and bonding process to prepare the SH $\rm TiO_2$ coating, respectively. The reinforced coating formed by this coating in continuous roughness improved the adhesion between the coating and the substrate, and could repeatedly produce super wettability after bearing mechanical stress.

As shown in Table 3, the dip coating method has the advantage characteristics of saving labor and materials, high production efficiency, simple equipment, and

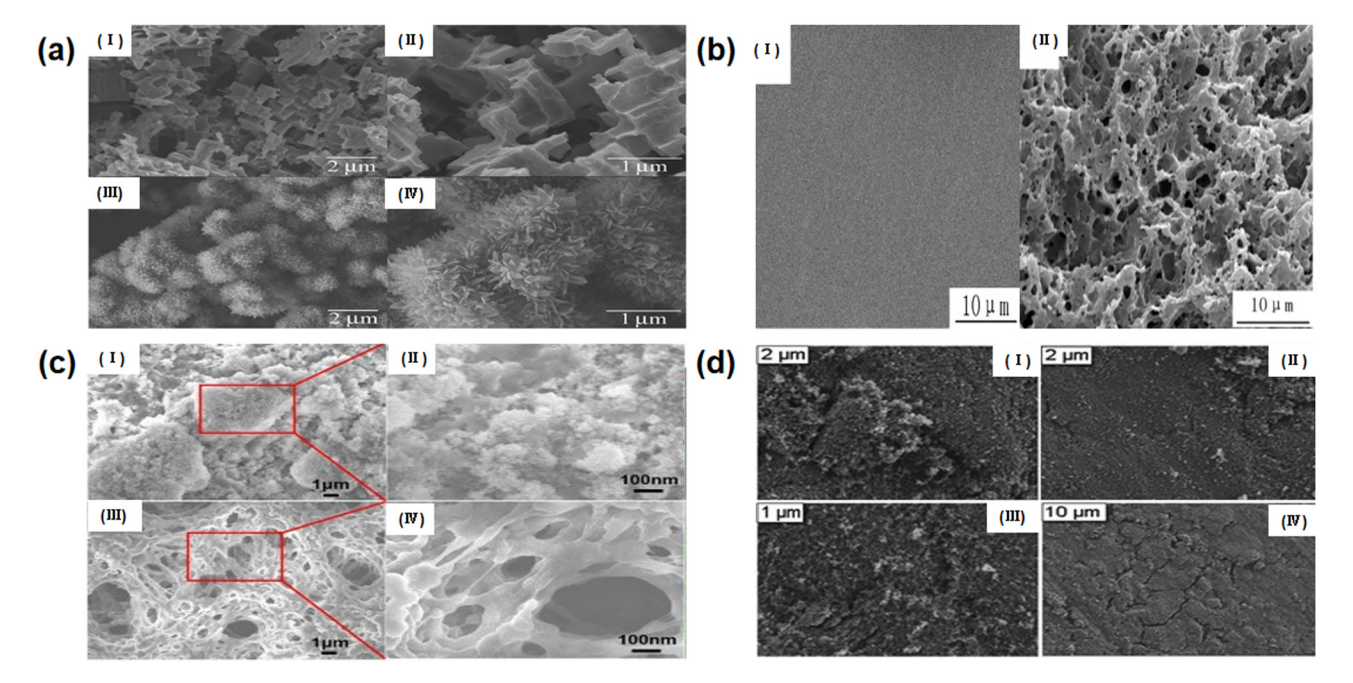


Figure 15: (a) SEM images of the Al surface prepared by (I–II) HCl etching and (III–IV) that treated in boiling water after etching [91], (b) (I) pure PVDF coating, (II) SH PVDF coating surface [92], (c) (I and II) PVDF coating, (III and IV) PVDF/SiO₂ coating [93], and (d) (I–IV) HRSEM morphology of SH-treated glass surface at different magnification [94].

[94]

[95]

References **Processing method** SA Type Contact angle Etching method Electrochemical etching of steel substrate 167.2 4.3 [67] Electrochemical etching of Al substrate 164 1.5 **[68]** Electrochemical etching of Mg-Al alloy 165.2 [69] 2 Chemical etching of Ni substrate 6.2 164 9 [74] Chemical etching of Al substrate 161.37 1 [75] Plasma etching of Si substrate 153.47 3.5 [80] Dip coating method FD-TMS/PDMS-TES coating 165 5 [91] 2 PVDF coating 156 **[92]** PVDF/SiO₂ coating 159 3 [93]

159

155

Table 3: Process parameters and SH properties of etching and dip coating methods

SiO₂ NPs SH coating

SiO₂/PVA/PAA/fluoropolymer hybrid coating

operation. It can adopt mechanization or automation for continuous production. The dip coating technique is most suitable for mass production with single variety. However, the fabricated surface should not have concave pattern of paint accumulation which could produce the defects including thin as well as uneven coating, and other disadvantages.

4.4 Mixing spray and combine spraying

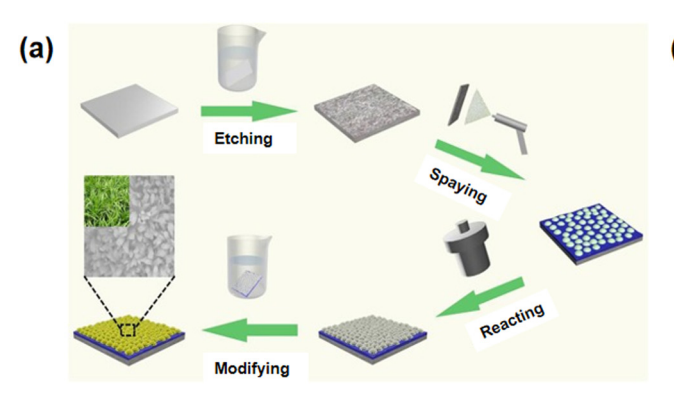
Spraying is one of micro/nano manufacturing methods. Spraying technique is depositing micron or nano particles with low surface energy on the substrate surface to form a rough structure. The sprayed surface has superhydrophobic properties. The spraying method has the advantages of simple operation, wide application range, low equipment cost, and large-scale production (Figure 16). It has been widely applied in the preparation of SH anticing/deicing coatings.

The solution in the spray prepared coating can be prepared by simple mixing, and the preparation operation of coating is relatively simple. Zeng *et al.* [98] mixed perfluoropolyether (PFPE) and ZnO and sprayed them on the glass (Figure 17(a)). The addition of PFPE reduced the coated surface energy from 18.12 mJ/m² at 0% to 13.22 mJ/m² at 15%. There was a linear relationship between the surface free energy and ice binding force. The coating with the highest contact angle of 158° and SA of 2° could be obtained, the freezing delay time could reach 107.1 s, and the freezing adhesion was reduced to 0.59 N which presented good anti-/deicing performance. Pan *et al.* [99] mixed dichloropentafluoropropane solvent (Asahiklin 225), 1*H*, 1*H*, 2*H*, 2*H*-hperfluorohexyltrichlorosilane (PFTS), and *n*-butyl cyanoacrylate (*n*-BCA) onto PDMS substrate to fabricate the coating with high contact angle of more than 150° and SA of 0°.

6

5

Jiang *et al.* [100] sprayed PVDF/CNTs mixed solution on the surface of Se cured strontium, and heated the coating to increase the bonding strength among surface particles. After treatment with FAS-17, the WCA of the coating was 163°, the icing delay time was increased to 584 s, and the ice adhesion was as low as 13.2 kPa. Due to the continuous



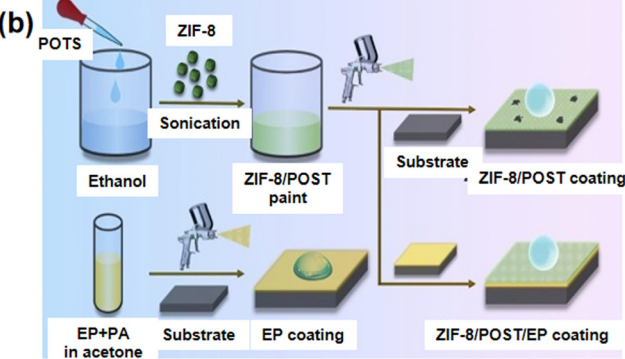


Figure 16: (a) Schematic of cluster ZnO coating preparation process [109], and (b) preparation of EP coating, SH ZIF-8/POTS coating, and ZIF-8/POTS/EP coating [113].

network formed by PVDF melt during heating, it could maintain excellent anti-icing performance even after severe mechanical wear and chemical corrosion. Yin *et al.* [101] mixed SiO₂ NPs, ethanol, and polytetrafluoroethylene (PTFE), and loaded the obtained suspension onto the copper mesh/Cu composite samples by spraying. The prepared coating samples had a WCA of more than 150°.

Liu et al. [102] used azodiisobutyronitrile to initiate the polymerization of acrylate monomer and perfluorooctyl methacrylate to prepare fluoro-modified polyacrylate (FPA). The FPA polymer was fully mixed with ECNTs in mortar and the mixture was dispersed in solvent. After spraying, the micro/nano structure composed of FPA and ECNTs was formatted, which gave PESC stable superhydrophobicity, and the WCA was increased to 150°. Jiang et al. [103] applied the combination of inorganic particles and carbon nanotubes (CNTs) to spray onto the substrate to prepare an anti-icing coating with micro/nano composite materials. The WCA of the coating was 161°, and the ice adhesion was as low as 2.65 kPa. Xie et al. [104] coated the attapulgite nanorods with polypyrrole through the oxidative polymerization of pyrrole, and then coated the attapulgite nanorods with cetylpolysiloxane through hydrolysis condensation. A photothermal superhydrophobic coating was manufactured by spraying the mixture of modified attapulgite suspension and silicone resin on aluminum plate. The WCA of the coating was 162.7°, and the SA was 2.7°.

The SH coatings with different properties can be fabricated through controlling the spraying pressure and spraying sequence. Xue *et al.* [105] prepared the superhydrophobic

photothermal coating with anti-icing performance by sequentially spraying cuttlefish juice melanin and ${\rm SiO_2}$ NPs. Due to the black pigment in cuttlefish juice, the coating showed high photothermal conversion performance. The freezing time of water droplets on the surface was delayed to 144 s, which was five times that of ordinary glass. The adhesion strength of ice was reduced to 25.65 kPa.

Li et al. [106] sprayed the SH suspension prepared from fluorinated epoxy resin and PTFE particles on the glass substrate with a spraying pressure of 0.25~2 bar to control the surface morphology of tunable adhesion superhydrophobic coating (TASC). The anti-icing properties of TASCs with different surface morphologies and roughness were investigated by freezing time and ice adhesion strength. Compared with TASC-0.25, the TASC-2.0 showed excellent anti-icing performance with freezing time of 392 s and ice adhesion strength of 51 kPa. Xie et al. [107] proposed waterborne polyurethane acute solution and hexadecyl polysiloxane modified diatomaceous earth acute suspension were successively sprayed on glass, Al alloy plate, Mg alloy plate, and other substrates, respectively. The coating had SH properties with contact angle of 168.1° and SA of about 4.9°. Compared with the bare substrate, it significantly increased the icing time to 361 s, and the icing strength at -15°C was decreased to 73.9 kPa. Zeng et al. [108] combined hydrophobically modified epoxy resin matrix with micro/nano fluoropolymer particles (Figure 16(b)). The superhydrophobic coating was prepared by multi-layer spraying with EP as adhesive. The maximum contact angle and minimum SA

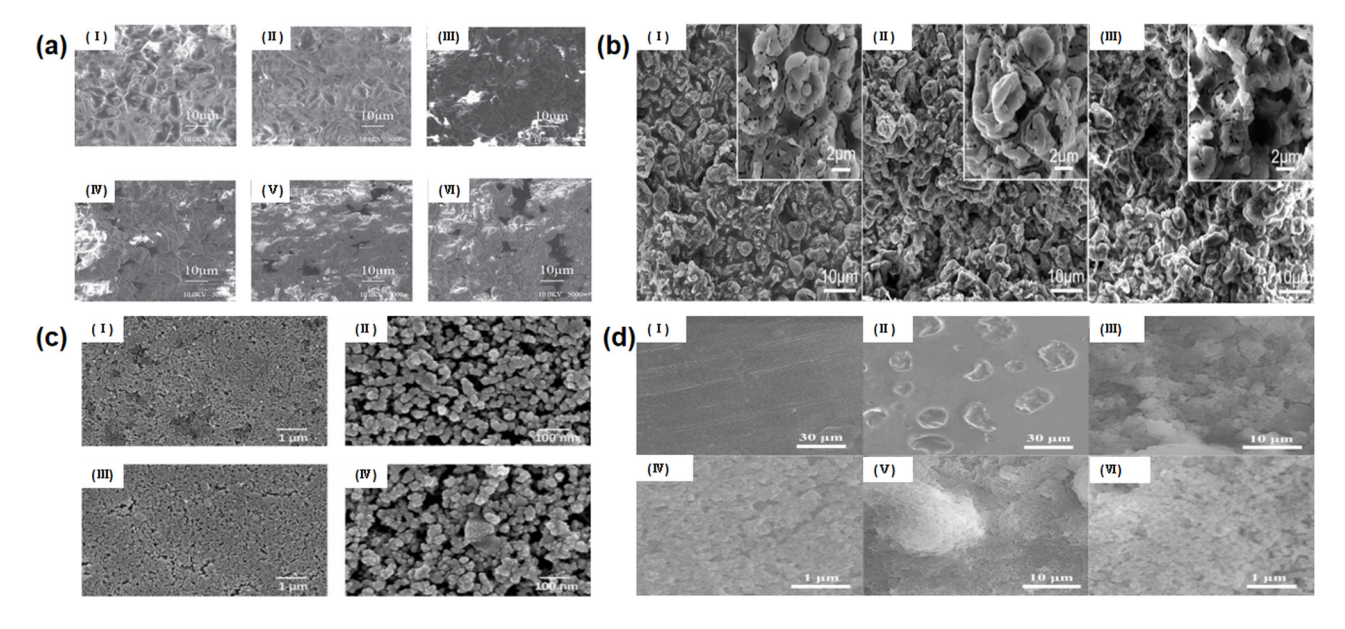


Figure 17: (a) (I–VI) Micro morphology of coatings with different ZnO content (0, 2, 4, 6, 8, 10%) [98], (b) SEM images of FP/FSEP coating: (I) FP-100%, (II) FP-200%, and (III) FP-300% [108], (c) SEM images of (I) bare magnesium alloy, (II) etched magnesium alloy (III and IV) clustered ZnO/EP surface [112], and (d) SEM images of (I) Q235 steel, (II) EP coating, (III and IV) ZIF-8/POTS coating, and (V and VI) ZIF-8/POTS/EP coating [116].

of the coating were 160° and 2°, respectively, and its SH properties were maintained even after 240 wear cycles and 360 s sandblasting. The coating had good corrosion resistance and self-cleaning performance, too.

Zheng et al. [109] prepared a magnetically responsive flexible SH photothermal film (PFe-PCS) composed of PDMS, iron powder, and candle smoke by spraying technique. The coating had good superhydrophobicity with a WCA of up to 154.5° and a SA as low as 3.13°. The PFe-PCS membrane could be folded repeatedly from 0° to 180°. No delamination or cracking was observed after 500 folding cycles, which showed that the sample had good flexibility and fatigue resistance. Yin et al. [110] fabricated the micro/nano polyhedral oligomeric silsesquioxane/PDMS (POSS/PDMS) composite coating with a similar spraying technique. When the POSS content exceeded 5%, a spherical/cylindrical micro/ nano structure was formatted, which made the POSS increase concentration and spray cycle times by fourfold, and could significantly reduce the distance between the particles. This spatial geometry embedded in the interphase hollow structure combined an effective heat transfer barrier, which made the surface wettability and ice adhesion greatly reduce. It caused the water freezing temperature to reduce to -26.3°C.

In the preparation of SH coatings by spraying, other manufacturing methods such as chemical etching and grafting can be combined to obtain more excellent hydrophobic properties. Shen et al. [111] chemically etched the aluminum plate in HCl solution. They sprayed the fluorinated SiO₂ NPs on the PDMS coating substrate after curing to obtain an SH surface with a contact angle of 155.3°. The results indicated that the delayed icing performance was extended from 4.8 to 276.2 s of bare aluminum. Zhou et al. [112] etched Mg alloy in HCl, sprayed ZnO seeds and placed them in ZnO growth solution to prepare cluster ZnO coating composed of interdigital ZnO rods (Figure 16(c)). After modification with stearic acid, the coating showed SH properties, and the contact angle was 163°. The coating showed excellent wear resistance and corrosion resistance. Wu et al. [113] sprayed SiO2 NPs onto glass fiber reinforced epoxy (GFRE) substrate to obtain superhydrophobic coating. The ice adhesion value of SiO₂ NPs coating was about 64.7 ± 5.4 kPa. After ultraviolet weathering and sand erosion, the ice adhesion strength was still less than 100 kPa.

Brown *et al.* [114] prepared a SH double-layer coating composed of thick TiO₂ coating deposited by plasma spraying and thin coating deposited by CVD. The coating presented a contact angle of 159° and a CAH of 3.8°. Zhu *et al.* [115] sprayed PDMS/TiO₂ NPs onto the surface of pre-deposited PDMS micron particles to fabricate a micro/nano hierarchical structure, and prepared a SH anti-icing coating with reversible wettability and durability. The WCA of SH anti-icing coated

surface was up to 168.6°, and the adhesion was as low as 4 μ N. The freezing time of droplets was extended to 895 s.

Chen et al. [116] sprayed EP coating on the surface of substrate, and then sprayed it after curing. The ZiF-8 NPs modified by 1H,1H,2H-2H perfluorooctyltriethoxysilane (POTS) were used to prepare SH coating with contact angle of about 168.2° and SA of about 2° (Figure 16(d)). Xie [117] prepared a SH coating bydirectly spraying APTES treated silica/ethanol suspension onto a steel substrate. Xie [117] prepared a SH coating by directly spraying APTES treated silica/ethanol suspension onto a steel substrate. Its WCA exceeded 150°. Ma et al. [118] dispersed PFEPx system and FCNTs in acetone, and the mass score of PFEP and FCNTs was named as PFEPx FCNTsy (y referred to as the content of FCNTs in PFEP). The surface roughness could be adjusted by grafting CNTs with perfluorinated segments and flexible spacer groups (FCNTs). The mixed solution was sprayed on the substrate to prepare SH coating. Among them, the PFEP30/ FCNTs40 had the best water repellent performance with a contact angle of about 152° and SA of about 5°. Wang et al. [119] designed a perfluorododecylated graphene nanoribbon film, which was applied by spraying method. Due to both the low polarizability of perfluorinated carbons and the intrinsic conductive nature of graphene nanoribbons, the film had SH properties and deicing performance by applied voltage heating. Guo et al. [120] prepared a photothermal effect anti-/deicing coating by combining photothermal carbon nanofibers with PDMS and polyvinylpyrrolidone. Compared with the films, there was 34-fold increase in freezing delay time, and the ice adhesion strength was reduced by 18 kPa.

The spraying technique has been widely applied. However, it usually has poor adhesion between coating and substrate and low durability of SH surface (Table 4). The manufacturing chains are complex, and the change in process parameters has great impact on the performance of finished products. It is often required to carry out various treatments on the surface to be sprayed to ensure the adhesion of spraying medium.

4.5 Chemical grafting and coupling grafting

Grafting is a micro/nano manufacturing method that reacts with the surface components of polymer through chemical reagents to produce active centers, so as to trigger the polymerization of monomers. The grafting usually introduces the energy substance on the bottom surface into the substrate surface or forms a special micro/nano structure to obtain SH and anti-/deicing performance (Figure 18).

Fenero et al. [121] prepared layered micro/nanostructures by chemical etching to induce SH. To reduce its

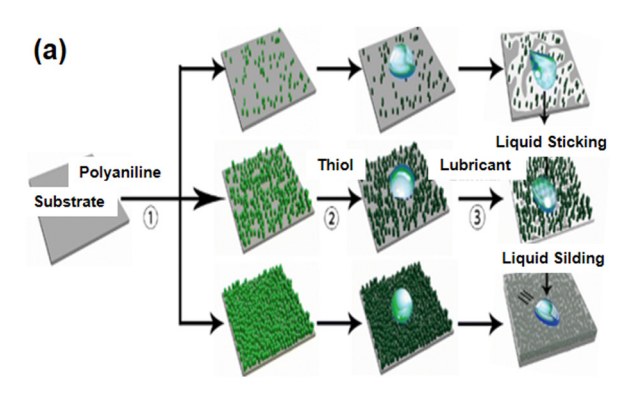
Table 4: Characteristics and parameters of spraying method

Author	Spray solution	Substrate	Contact angle	SA	Other features
Zeng <i>et al.</i> [98]	PFPE and ZnO mixed	Glass	158°	2°	The content of PFPE is 15% and the content of ZnO is 6 wt%, the performance is the best
Pan <i>et al.</i> [99]	Chloropentafluoropropane solvent mixed with PFTS and <i>n</i> -BCA	PDMS	>150°	~0°	It has strong repellency to solvents, acid-base and polymer solutions
Xie <i>et al.</i> [104]	Mixture of modified attapulgite suspension and silicone resin	Al	162.7°	2.7°	Synergistic effect of excellent photothermal performance and good stability
Xie <i>et al.</i> [107]	Aqueous polyurethane aqueous solution and cetylpolysiloxane modified DE aqueous suspension	Glass and others	168.1 ± 1.6°	4.9 ± 0.7°	Excellent mechanical, chemical, and environmental stability
Zeng et al. [108]	Micro/nano fluoropolymer particles	Metal substrate	160°	2°	Wear resistance, corrosion resistance, self-cleaning
Zheng et al. [109]	Iron powder, PDMS, and candle soot	Glass	154.5°	3.13°	Good flexibility and fatigue resistance
Chen <i>et al.</i> [116]	POTS, ZIF-8 NPs	Cu, glass, and others	168.2°	2°	Good self-cleaning performance

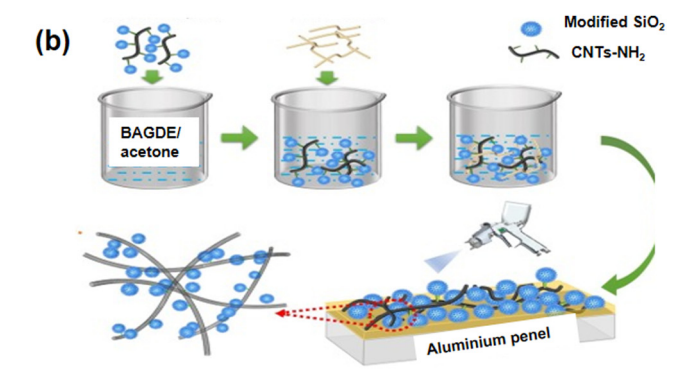
surface free energy, the PFPE was grafted onto corrugated Al substrate and the system was flooded. The surface presented SH characteristics, and the WCA was 160°. In addition, the floodlit surface significantly delayed the freezing time of water droplets to 5,100 s, which was about 20 times that of original aluminum (260 s). Yu *et al.* [122] grafted polyaniline nanofibers onto glass plates by oxidative polymerization, and used perfluoroalkyl mercaptan modification and PFPE lubricant penetration to fabricate the slippery lubricant-infused porous surfaces (as shown in Figure 18(a)). After treatment, the surface WCA was about 153° and the water SA was about 5° (Figure 19(a)). Li *et al.* [123] grafted SI-eATRP of methacryl-POSS (MA-POSS) on cotton and reacted with Michael addition of 1*H*,1*H*,2*H*,2*H*-perfluorododecyl-1-thiol (PFDT) through amine catalyzed thiol- MA-

POSS to prepare durable MA-POSS-PFDT coating. After fluorination, the WCA was increased to about 160° and the water SA was about 10°.

Zhang et al. [124] prepared CNTs-SiO₂ hybrid by grafting silica NPs onto CNTs to manufacture epoxy matrix based SH coating (Figure 19(b)). The surface morphology, roughness, and wettability of CNTs-SiO₂/epoxy coating could be adjusted by controlling the ratio of CNTs to SiO₂. The CNTs-SiO₂/epoxy coating had SH characteristics and significant photothermal conversion ability of CNTs (Figure 19(b)). Under laser irradiation, it could significantly delay the freezing time of water and effectively melt the ice in a few seconds. Gao et al. [125] prepared micro/nanostructured metal organic framework (MOF) coating (LIMNSMC) by fixing lubricating fluid with porous micro/nano structure coated with MOF. The prepared coating







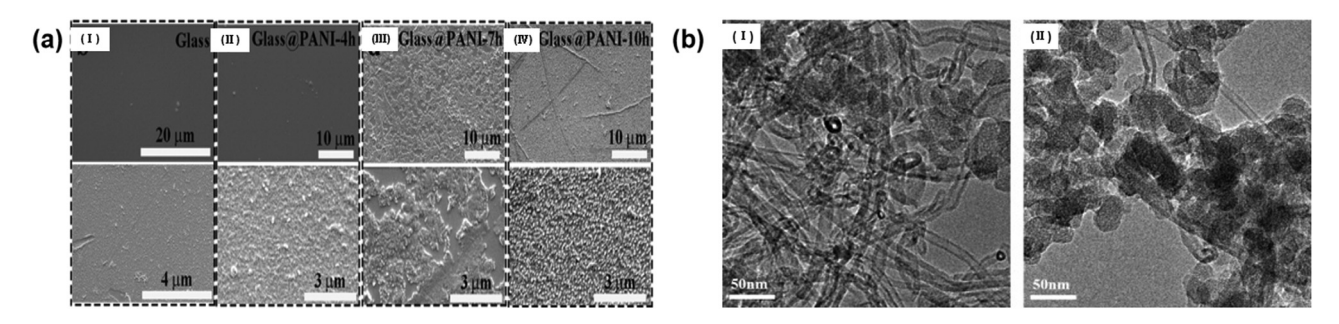


Figure 19: (a) SEM images of glass surface (I-IV) after different time grafting treatments [122], and (b) (I-II) SEM images of CNTs-SiO₂ grafted surface [124].

exhibits high ice resistance, with a freezing temperature of approximately –39°C for condensed water on the coating and an ice adhesion strength of approximately 10 kPa. The high ice resistance of LIMNSMC could be maintained in ten freezing/melting cycles and six anti-icing/deicing cycles, indicating that the coating has good durability.

Zhan et al. [126] linked fluoropolymers to silica NPs through free radical polymerization. It had controllable molecular design, excellent thermal stability, and high SH. The WCA up to 170.3° and the CAH less than 3° could effectively promote the removal of droplets. Zhang et al. [127] synthesized nanoscale thickness MOF coating (NTMC) on polypropylene (PP) substrate, and grafted silane coupling agent KH560 onto NTMC to form KH560-NTMC. The hydrogen terminated silicone fluid was grafted onto KH560-NTMC to prepare self-lubricating MOF coating (SLNTMC). The WCA of KH560-NTMC coating was 84.6°, and that of SLNTMC was 133.2°. Because the silicone layer SLNTMC covered the ice nucleation sites of ice and reduced the binding force of water/ice, the SLNTMC could reduce the binding force of ice to 9.4 kPa and maintain low icing adhesion after 20 anti-/deicing cycles, which indicated that the SLNTMC had good durability.

It is shown that the grafted product is stable, has good surface properties, wide processing range, and good wear resistance. However, the grafting process is not suitable in mass production due to its long reaction time, low efficiency, and high production cost.

4.6 Organic material template and metal template

Template method is to take the material with micro/nano rough structure or low surface energy as the template, and to deposit the relevant materials into the holes or surfaces of the template through physical or chemical processing (Figure 20). The template is then removed to obtain the nano materials with the standard morphology and size of

the template. This micro/nano manufacturing method can be applied to fabricate material surface with SH properties.

Yin *et al.* [128] assembled polystyrene (PS) microspheres into a compact opal crystal template, and then poured the mixed solution of Fe_3O_4 NPs silicone predictor onto the template. After solidifying and removing the template, the coating was fluorinated to form an inverse opal porous PDMS film with evenly distributed Fe_3O_4 NPs. The ice adhesion strength of fluorinated porous film infiltrated with perfluoro polyether (Krytox from Dupont) lubricant (LF) was about 25 kPa.

Song et al. [129] fabricated a super hydrophobic column array with a diameter of 1.05 mm, a height of 0.8 mm, and a spacing of 0.25 mm. They observed typical pancake bounce and reduced the contact time with the surface by 57.8%. The pillar arrays with millimeter diameter and height-to-diameter ratio of <1 can be easily manufactured on a large area. Shao et al. [130] prepared shape memory polyurethane surface with shape memory effect through aluminum template. Due to the special hierarchical structure, the surface showed typical lotus effect and presented SH properties (contact angle 154 \pm 2°, SA 3 \pm 1°). After the vertical microstructure was crushed by external pressure, the contact angle of the material surface was 151°, and the SA was greater than 180°. It showed high viscosity. After heating at 50°C for 5 min, the original microstructure was restored, and the transformation from "lotus leaf effect" to "rose petal effect" was realized.

Yuan *et al.* [131] used PDMS as an intermediate mold as a soft copy to transfer T-shaped overhanging microstructures on silicon and dual resist masters to curable materials to form a SH surface with a WCA greater than 150°. Su *et al.* [132] coated porous Al template with ethyl acetate solution containing 0.5 wt% PU precursor to prepare SH membrane. The contact angle of water droplets on the SH membrane was $166.3 \pm 2.41^\circ$.

As shown in Table 5, the template method has the advantages of simple processing, low requirements for process parameters, repeatability, and reproducibility. However,

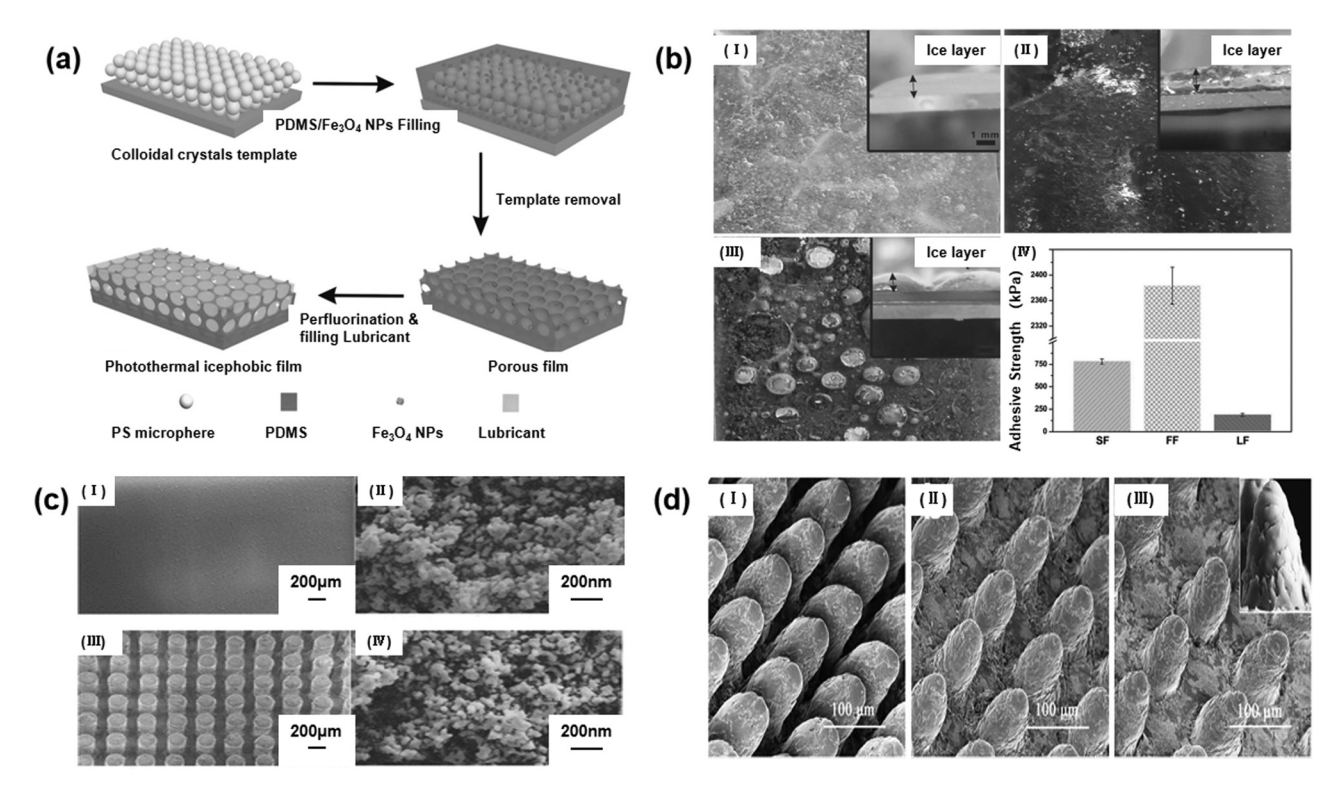


Figure 20: (a) Fabrication procedures of a model surface. (b) Ice formation and the adhesion characteristics: Lubricant (SF, I), fluorinated porous film (FF, II), porous film (PF, III), and the average ice adhesion strength on different films (IV) [128]. (c) SEM images of (I and II) SH plane. (III and IV) SH column arrays with d = 0.3 mm, s = 0.2 mm, and h = 1 mm [129]. (d) SEM images of duplicate surfaces with different column spacings: (I) 80 μm, (II) 100 μm, and (III) 120 μm [130].

the coating/surface prepared by template method has poor durability and the manufacturing cost is high. In the separation process, it may damage the surface micro/nano structure and reduce its performance.

4.7 Silicon compound sol-gel coating

In the sol-gel method, the compounds containing high chemically active components are used as precursors. These raw materials are uniformly mixed in the liquid phase, and the hydrolysis and condensation chemical reactions are carried out to form a stable transparent sol system in the

solution (Figure 21). The sol is slowly polymerized between aged colloidal particles to form a three-dimensional network structure of gel. The gel network is filled with solvent that has lost fluidity to form a gel. After drying, sintering, and curing, the gel can be used to prepare molecular and nano substructure materials.

Wu et al. [133] prepared TEOS and GLYMO sols by sol–gel method. The SiO_2 NPs with particle size of 10–20 nm treated by perfluorooctyltriethoxysilane were added as reinforcements and sprayed onto GFRE substrate. The synthesized surface presented a contact angle of up to 166°. Ke et al. [134] mixed tetraethyl orthosilicate and hydrochloric acid through sol–gel technology to prepare $Si(OH)_4$ sol, and mixed different amounts of $Si(OH)_4$ sol with SiO_2 suspension. The above

Table 5: Performance parameters and advantages of coating/surface prepared by template method

Ref.	Prepared surface or coating	Contact angle	Advantage
Yin <i>et al.</i> [128]	Porous PDMS membrane	>150°	Photothermal effect can melt ice in a short time
Song <i>et al.</i> [129]	Al template columnar array surface	>155°	Pancake bounce on super hydrophobic column array
Shao <i>et al.</i> [130]	Polyurethane surface	151°	Shape memory effect with thermal response
Yuan et al. [131]	T-shaped suspension microstructure on PDMS	>150°	Chemical inertness, scalability, flexibility and transparency.
Su <i>et al.</i> [132]	SH surface composed of PU elastomer	165.1°	High wear resistance

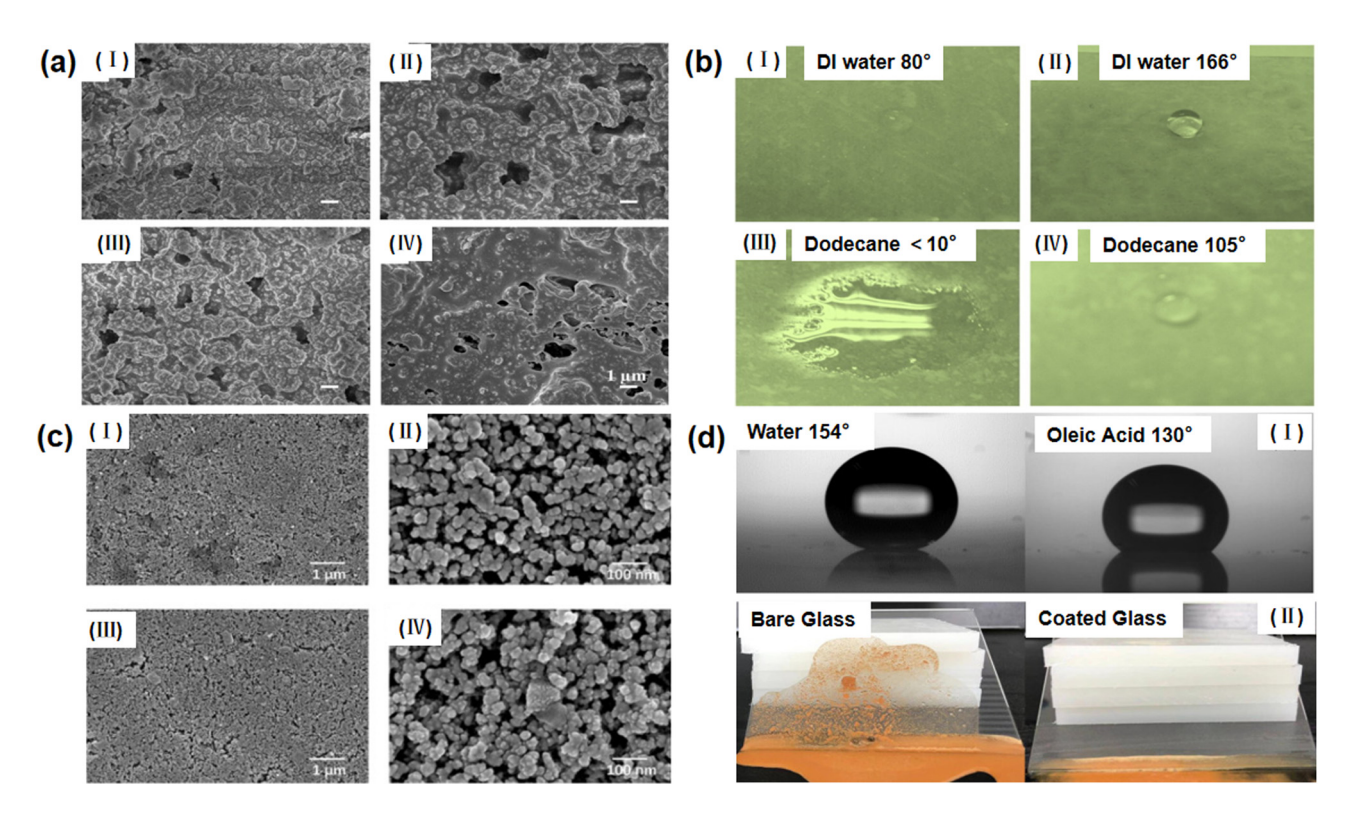


Figure 21: (a) (I–IV) FE-SEM images of SiO_2 nanoparticles with different concentrations enhancing the surface of coatings [133], (b) water and dodecane droplets drop on the uncoated (I and III) and coated (II and IV) GFRE substrates, respectively [133], (c) SEM images of SiO_2 NPs (I–II) and $Si(OH)_4$ (III–IV) sol coatings with different loading amounts [134], and (d) images of water (I) and oleic acid (II) droplets on acoating made of 1.5:1.31 SiO_2 and $Si(OH)_4$ [134].

mixture with 1 mL was dropped on a clean glass substrate and coated with a 10 μm Mayer rod to obtain a coating with micro/nano layered roughness. When introduced 1.5 g SiO₂ NPs, the WCA of the coating was 154°, which presented superhydrophobicity.

Cai *et al.* [135] prepared the superhydrophobic coating of silica NPs modified by methyltrimethoxysilane, ethyltriethoxysilane, and 1*H*,1*H*,2*H*,2*H*-perfluorooctyltriethoxysilane (HFOTES) *via* the sol–gel process. The WCA could reach 150.2°, and the minimum water hysteresis was 3.3°. Eshaghi *et al.* [136] prepared composite films on glass substrates by sol–gel method using silica-silica nanotube nanocomposite, and soaked the samples in PFTS solution to modify the nanocomposite films. The silica nanotube/PFTS film increased the WCA of glass substrate from 16° to 152°. The icing test results showed that the superhydrophobic coating caused the icing time of glass surface to increase from 102 to 874 s.

The raw materials of the sol-gel method are first dispersed into the solvent to form a low viscosity solution. Therefore, the molecular level uniformity can be obtained in a very short time. Due to the solution reaction step, it

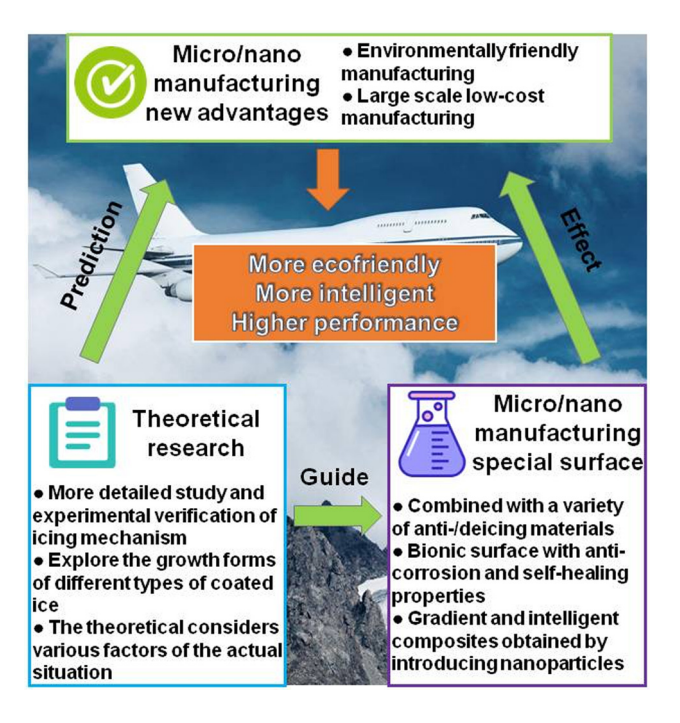


Figure 22: Potential research directions of micro/nano manufacture.

Table 6: Summary of micro/nano fabrication methods for anti-/deicing surfaces

Processing methods	Advantages	Disadvantages	Ref.
Etching method	Simple process and good surface performance	Surface modification required, long time	[64]–[78]
Deposition method	Suitable for complex surface machining	The coating is easy to wear and the structural stability is general	[79]–[87]
Dip coating method	Simple operation and high production efficiency	The substrate shall be flat and the coating may be uneven	[88]–[94]
Spraying method	Wide application range	Complex process parameters and general coating adhesion	[95]-[115]
Grafting method	Stable product and high abrasion resistance	Long time and low efficiency	[116]–[122]
Template method	Simple processing and high repeatability	Not easy to separate, micro/nano structure may be damaged	[123]–[127]
Sol-gel method	Uniform coating	Complex process and high cost	[128]-[131]

can uniformly and quantitatively add some trace elements to achieve uniform doping at the molecular level, and the reaction conditions are simple. However, the sol–gel processing of raw materials is complex, takes a long time, and is expensive.

4.8 Other surface modification methods

The wide application of micro/nano manufacturing in machining [137], microelectronics [138,139], and other fields shows that the diversified process can be employed to the field of anti-icing and deicing technology. Wu et al. [140] prepared a multifunctional SH coating by compounding iron oxide NPs (Fe₃O₄ NPs) with fluorinated epoxy resin through reverse osmosis process. The coating had excellent water repellency (WCA up to 161.0°, SA as low as 1.4°), and could maintain superhydrophobicity in 260 sandpaper abrasion. Because the special micro/nano structure greatly hindered the heat transfer, the freezing of water droplets was delayed by 35 min compared with that of the uncoated substrate under the same conditions. Due to the photothermal effect of Fe₃O₄ NPs, the surface temperature of the coating could quickly rise to more than 0°C under infrared radiation, which was conducive to the melting of ice on the cold surface.

Liao et al. [141] fabricated $\rm ZnO/SiO_2/PTFE$ sandwich nanostructures on the glass surface by RF magnetron sputtering. The fabricated nanostructure surface had a contact angle of 167.2° and a SA of less than 1°, which was due to the low surface energy of PTFE and micro/nano cavitation induced by rough nanostructures. After spraying in glazed ice for 120 min, only 17.9% of the prepared coating surface was frozen. In addition, due to the addition of $\rm SiO_2$ intermediate layer, the corrosion resistance and insulation properties of the prepared SHP were significantly improved. Zhu

et al. [142] prepared the anti-icing composite coating with phase change performance by adding phase-change microcapsules (PCMs) to room temperature vulcanized (RTV) or fluorosilicone (FS) copolymer. Because PCMs released a certain amount of latent heat during cooling, the composite coating could delay the freezing of water droplets on the coating surface. The ice shear strength on the RTV/PCM coating surface (102~132 kPa) was lower than that on the FS/PCM coating surface (378~489 kPa). The shape memory alloy (SMA) materials showed the ability to change shape and generate force through martensitic phase transformation [143]. After transferring appropriate energy to the material, the SMA can remove ice through unique surface bending, shearing, and other methods.

5 Conclusion

The micro/nano manufacturing technologies of anti-/deicing surface, the influence law of relevant process parameters on surface SH performance, and the improvement of surface energy and SH performance were reviewed. However, the mechanism of the effect of surface wettability on ice adhesion strength has not been unified. The ice adhesion strength values obtained under different experimental conditions are quite different. It is necessary to further improve the theory of micro/nano manufacturing on surface anti-icing and deicing performance. There are requirements for more in-depth research on the theory of surface icing adhesion strength and the influence law of relevant factors, to reveal the multi parameter coupling mechanism in micro/nano manufacturing. The theoretical foundation is urgently to be provided for industrialization to optimize design of micro/nano manufacturing antiicing and deicing surface.

The combination of various energy field assisted micro/ nano manufacturing methods can not only improve the accuracy of micro/nano manufacturing as well as the complexity of the process but also provide more feasible design space for the manufacturing of anti-/deicing micro/nano morphology (as shown in Figure 22). For instance, the micro/nano manufacturing method of electromagnetic field coupling with assisted local spray deposition can realize the processing of more high-precision complex morphology. The micro/nanostructures fabricated by femtosecond laser have great application potential in the fields of machinery, electronics, biosensors and drives, physics, and chemistry. Moreover, the introduction of NPs into alloy matrix materials to obtain gradient, amorphous, quasicrystal, and intelligent micro/nano manufacturing composites will be the development trend in future. Compared with one single nano material, the combination of nano materials and other methods (such as anodic oxidation, heat treatment, vibration polishing, etc.) can effectively improve the comprehensive properties of the alloys.

The icing application of SH coating is in the stage of focusing on the superficial discussion and analysis of the experimental results. The multidisciplinary methods including theoretical simulation and calculation as well as experimental methods from the perspective of thermodynamics and dynamics analysis need to be investigated for the design of micro/nano manufacturing SH coatings. Further research on the mechanism and system theory of micro/nano surface icing and anti-/deicing is challenged. In addition, the SH coatings with self-healing and self-healing will be paid more attention to aircraft applications, and the SH surface made of micro/nano materials to restore SH properties will greatly extend the service life of aircrafts.

The new intelligent SH coating has been proposed. The intelligent coating contains corrosion inhibitor and self-healing ability, so it can independently repair its anti-corrosion, anti-biofouling, and self-healing functions. This intelligent multifunctional integrated coating is expected to be combined with micro/nano functional surfaces to achieve wide industrial applications.

The in-depth systematic research and experimental verification are still needed in the application of aircraft anti-icing and deicing models (Table 6). To meet the challenges of flight safety guarantee under extreme conditions, it is necessary to further improve and put forward the research system of aircraft anti-icing and deicing surface design, micro/nano manufacturing, and experimental verification. The improvement in the accuracy and efficiency of micro/nano manufacturing of anti-icing and deicing surface, and the decrease in the micro/nano manufacturing cost can make it more applicable in aerospace industries.

Funding information: This work was supported by Key Laboratory of Icing and Anti/Deicing of CARDC (Grant No. IADL20210407), Natural Foundation of Shandong Province (Grant No. ZR2019BEE068), and Guangdong Basic and Applied Basic Research Foundation (Grant No. 2020A1515111208). The authors thank the referees of this article for their valuable and very helpful comments.

Author contributions: All authors have accepted responsibility for the entire content of this manuscript and approved its submission.

Conflict of interest: The authors state no conflict of interest.

References

- [1] Politovich MK. Aircraft icing. Encyc Atmosp Sci. 2003;358:68–75.
- [2] Ayra ES, Rodríguez Sanz Á, Arnaldo Valdés R, Gómez Comendador F, Cano J. Detection and warning of ice crystals clogging pitot probes from total air temperature anomalies. Aerosp Sci Technol. 2020;102:105874. doi: 10.1016/j.ast.2020.105874.
- [3] Mason J, Grzych ML, Chow P Current perspectives on jet engine power loss in ice crystal conditions: Engine icing (AIAA Atmosp. Sp. Environ. 7th AIRA Res. Imp. Forum, 2008).
- [4] Cao YH, Tan WY, Wu Z. Aircraft icing: An ongoing threat to aviation safety. Aerosp Sci Technol. 2018;75:353–85. doi: 10.1016/j.ast. 2017 12 028.
- [5] Bank of East Asia Ltd. Final Report on the Accident on 1st June 2009 to the Airbus A330-203 Registered F-GZCP Operated by Air France Flight AF 447 Rio de Janeiro-Paris (BEA, 2012).
- [6] Lv J, Song Y, Jiang L, Wang J. Bio-inspired strategies for anti-icing. ACS Nano. 2014;8:3152–69. doi: 10.1021/nn406522n.
- [7] Wei K, Yang Y, Zuo H, Zhong D. A review on ice detection technology and ice elimination technology for wind turbine. Wind Energy. 2020;23:433–57. doi: 10.1002/we.2427.
- [8] Kreder MJ, Alvarenga J, Kim P, Aizenberg J. Design of anti-icing surfaces: smooth, textured or slippery? Nat Rev Mater. 2016;1:1–15. doi: 10.1038/natrevmats.2015.3.
- [9] Manoharan K, Bhattacharya S. Superhydrophobic surfaces review: Functional application, fabrication techniques and limitations.
 J Micromanuf. 2019;2:59–78. doi: 10.1177/2516598419836345.
- [10] Alamri S, Vercillo VI, Aguilar-Morales A, Schell F, Wetterwald M, Lasagni AF, et al. Self-limited ice formation and efficient de-icing on superhydrophobic micro-structured airfoils through direct laser interference patterning. Adv Mater Int. 2020;7:2001231. doi: 10.1002/admi.202001231.
- [11] Yancheshme AA, Momen G, Aminabadi RJ. Mechanisms of ice formation and propagation on superhydrophobic surfaces: A review. Adv Colloid Interface Sci. 2020;279:102155. doi: 10.1016/j. cis 2020 102155
- [12] Gibbs JW. On the equilibrium of heterogeneous substances. Am J Sci. 1879;3:300–20. doi: 10.2475/ajs.s3-16.96.441.
- [13] Markov IV. Crystal growth for beginners: fundamentals of nucleation, crystal growth and epitaxy. Hackensack: World scientific Publishing Co. Pte. Ltd.; Vol. 14, 2016.

- [14] Dhanaraj G, Byrappa K, Prasad VV, et al. Springer handbook of crystal growth. Heidelberg: Springer; 2010. p. 3-16.
- [15] Fletcher NH. Size effect in heterogeneous nucleation. J chem phys. 1958;29:572-6. doi: 10.1063/1.1744540.
- [16] Ketcham WM, Hobbs PV. An experimental determination of the surface energies of ice. Philos Mag. 1969;19:1161-73. doi: 10.1080/ 14786436908228641.
- [17] Iraiizad P. Nazifi S. Ghasemi H. Icephobic surfaces: Definition and figures of merit. Adv Colloid Interface Sci. 2019;269:203-18. doi: 10.1016/j.cis.2019.04.005.
- [18] Boreyko JB, Chen CH. Self-propelled dropwise condensate on superhydrophobic surfaces. Phys Rev Lett. 2009;103:184501. doi: 10.1103/PhysRevLett.103.184501.
- [19] Tourkine P. Le MM. Quéré D. Delayed freezing on water repellent materials. Langmuir. 2009;25:7214-6. doi: 10.1021/la900929u.
- [20] Alizadeh A, Yamada M, Li R, Shang W, Otta S, Zhong S, et al. Dynamics of ice nucleation on water repellent surfaces. Langmuir. 2012;28:3180-6. doi: 10.1021/la2045256.
- Park C, Kim T, Kim YI, Lee MW, An S, Yoon SS. Supersonically sprayed transparent flexible multifunctional composites for selfcleaning, anti-icing, anti-fogging, and anti-bacterial applications. Compos Pt B-Eng. 2021;222:109070. doi: 10.1016/j.compositesb. 2021.109070.
- [22] Tong W, Xiong D, Wang N, Wu Z, Zhou H. Mechanically robust superhydrophobic coating for aeronautical composite against ice accretion and ice adhesion. Compos Pt B-Eng. 2019;176:107267. doi: 10.1016/j.compositesb.2019.107267.
- Wang F, Ding W, He J, Zhang Z. Phase transition enabled durable [23] anti-icing surfaces and its DIY design. Chem Eng J. 2019;360:243-9. doi: 10.1016/j.cej.2018.11.224.
- [24] Fu QT, Liu EJ, Wilson P, Chen Z. Ice nucleation behaviour on solgel coatings with different surface energy and roughness. Phys Chem Chem Phys. 2015;17:21492-500. doi: 10.1039/C5CP03243A.
- [25] Ruan M, Li W, Wang B, Deng B, Ma F, Yu Z. Preparation and antiicing behavior of superhydrophobic surfaces on aluminum alloy substrates. Langmuir. 2013;29:8482-91. doi: 10.1021/la400979d.
- [26] Wang Y, Zhao P. Temperature-based analysis of droplet cooling and freezing on femtosecond laser textured surfaces. Appl Therm Eng. 2022;206:118046. doi: 10.1016/j.applthermaleng.2022.118046.
- [27] Ly FY, Zhang P. Fabrication and characterization of superhydrophobic surfaces on aluminum alloy substrates. Appl Surf Sci. 2014;321:166-72. doi: 10.1016/j.apsusc.2014.09.147.
- [28] Namdari N, Otto GJ, Guo G, Sojoudi H, Rizvi R. Nanotextured surfaces with enhanced ice-traction and wear-resistance. Compos Pt B-Eng. 2022;238:109916. doi: 10.1016/j.compositesb.2022. 109916.
- [29] Ruan M, Zhan Y, Wu Y, Wang X, Li W, Chen Y, et al. Preparation of PTFE/PDMS superhydrophobic coating and its anti-icing performance. RSC Adv. 2017;7:41339-44. doi: 10.1039/C7RA05264B.
- [30] Wen M, Wang L, Zhang M, Jiang L, Zheng Y. Antifogging and icingdelay properties of composite micro-and nanostructured surfaces. ACS Appl Mater Interfaces. 2014;6:3963-8. doi: 10.1021/ am405232e.
- [31] Rahimi M, Afshari A, Thormann E. Effect of aluminum substrate surface modification on wettability and freezing delay of water droplet at subzero temperatures. ACS Appl Mater Interfaces. 2016;8:11147-53. doi: 10.1021/acsami.6b02321.
- [32] Shen Y, Tao H, Chen S, Zhu L, Wang T, Tao J. Icephobic/anti-icing potential of superhydrophobic Ti6Al4V surfaces with hierarchical textures. Rsc Adv. 2015;5:1666-72. doi: 10.1039/c4ra12150c.

- [33] Zuo Z, Liao R, Guo C, Yuan Y, Zhao X, Zhuang A, et al. Fabrication and anti-icing property of coral-like superhydrophobic aluminum surface. Appl Surf Sci. 2015;331:132-9. doi: 10.1016/j.apsusc.2015.
- [34] He M, Wang J, Li H, Song Y. Super-hydrophobic surfaces to condensed micro-droplets at temperatures below the freezing point retard ice/frost formation. Soft Matter. 2011;7:3993-4000. doi: 10.1039/C0SM01504K.
- Zhang Y, Klittich MR, Gao M, Dhinojwala A. Delaying frost for-[35] mation by controlling surface chemistry of carbon nanotubecoated steel surfaces. ACS Appl Mater Interfaces. 2017;9:6512-9. doi: 10.1021/acsami.6b11531.
- Zuo Z, Liao R, Zhao X, Song X, Qiao Z, Guo C, et al. Anti-frosting performance of superhydrophobic surface with ZnO nanorods. Appl Therm Eng. 2017;110:39-48. doi: 10.1016/j.applthermaleng. 2016.08.145.
- [37] Zhang Q, He M, Zeng X, Li K, Cui D, Chen J, et al. Condensation mode determines the freezing of condensed water on solid surfaces. Soft Matter. 2012;8:8285-8. doi: 10.1039/C2SM26206A.
- [38] Chu F, Wu X, Wang L. Dynamic melting of freezing droplets on ultraslippery superhydrophobic surfaces. ACS Appl Mater Interfaces. 2017;9:8420-5. doi: 10.1021/acsami.6b16803.
- Kim J, Jeon J, Kim DR, Lee KS. Quantitative analysis of anti-freezing [39] characteristics of superhydrophobic surfaces according to initial ice nuclei formation time and freezing propagation velocity. Int J Heat Mass Transf. 2018;126:109-17. doi: 10.1016/j. ijheatmasstransfer.2018.06.023.
- [40] Rønneberg S, He J, Zhang Z. The need for standards in low ice adhesion surface research: a critical review. J Adhes Sci Technol. 2020;34:319-47. doi: 10.1080/01694243.2019.1679523.
- [41] Memon H, Liu J, De Focatiis DSA, Choi K, Hou X. Intrinsic dependence of ice adhesion strength on surface roughness. Surf Coat Technol. 2020;385:125382. doi: 10.1016/j.surfcoat.2020.125382.
- [42] Janjua ZA, Turnbull B, Choy KL, Pandis C, Liu J, Hou X, et al. Performance and durability tests of smart icephobic coatings to reduce ice adhesion. Appl Surf Sci. 2017;407:555-64. doi: 10.1016/ j.apsusc.2017.02.206.
- Kulinich SA, Farzaneh M. Ice adhesion on super-hydrophobic [43] surfaces. Appl Surf Sci. 2019;255:8153-7. doi: 10.1016/j.apsusc. 2009.05.033.
- Laforte C, Beisswenger A. Icephobic material centrifuge adhesion [44] test. Proceedings of the 11th International Workshop on Atmospheric Icing of Structures. Montreal, QC, Canada: IWAIS; 2005. pp. 12-6
- Wang C, Fuller T, Zhang W, Wynne KJ. Thickness dependence of [45] ice removal stress for a polydimethylsiloxane nanocomposite: Sylgard 184. Langmuir. 2014;30:12819-26. doi: 10.1021/la5030444.
- [46] Rønneberg S, Zhuo Y, Laforte C, He J, Zhang Z. Interlaboratory study of ice adhesion using different techniques. Coatings. 2019;9:678. doi: 10.3390/coatings9100678.
- Rønneberg S, Laforte C, Volat C, He J, Zhang Z. The effect of ice [47] type on ice adhesion. AIP Adv. 2019;9:055304. doi: 10.1063/1. 5086242.
- Armstrong T, Roberts B, Swithinbank C. Illustrated glossary of [48] snow and ice. Prog Phys Geogr. 1973;36:862-4. doi: 10.1177/ 0309133312455984.
- [49] Sojoudi H, Wang M, Boscher ND, McKinley GH, Gleason KK. Durable and scalable icephobic surfaces: similarities and distinctions from superhydrophobic surfaces. Soft matter. 2016;12:1938-63. doi: 10.1039/C5SM02295A.

- [50] Butt HJ, Golovko DS, Bonaccurso E. On the derivation of Young's equation for sessile drops: nonequilibrium effects due to evaporation. J Phys Chem B. 2017;111:5277-83. doi: 10.1021/ jp065348g.
- [51] Wenzel RN. Surface roughness and contact angle. J Phys Chem. 1949;53:1466-7. doi: 10.1021/j150474a015.
- Whyman G, Bormashenko E, Stein T. The rigorous derivation of [52] Young, Cassie-Baxter and Wenzel equations and the analysis of the contact angle hysteresis phenomenon. Chem Phys Lett. 2008;450:355-9. doi: 10.1016/j.cplett.2007.11.033.
- [53] Shen Y, Wang G, Tao J, Zhu C, Liu S, Jin M, et al. Anti-icing performance of superhydrophobic texture surfaces depending on reference environments. Adv Mater Interfaces. 2017;4:1700836. doi: 10.1002/admi.201700836.
- [54] Li S, Huang J, Chen Z, Chen G, Lai Y. A review on special wettability textiles: theoretical models, fabrication technologies and multifunctional applications. J Mater Chem A. 2017;5:31-55. doi: 10. 1039/C6TA07984A.
- Meuler AJ, McKinley GH, Cohen RE. Exploiting topographical texture to impart icephobicity. ACS Nano. 2010;4:7048-52. doi: 10. 1021/nn103214a.
- [56] Mangini D, Antonini C, Marengo M, Amirfazli A. Runback ice formation mechanism on hydrophilic and superhydrophobic surfaces. Cold Reg Sci Tech. 2015;109:53-60. doi: 10.1016/j. coldregions.2014.09.012.
- Sarshar MA, Swarctz C, Hunter S, Simpson J, Choi CH. Effects of [57] contact angle hysteresis on ice adhesion and growth on superhydrophobic surfaces under dynamic flow conditions. Colloid Polym Sci. 2013;291:427–35. doi: 10.1007/s00396-012-2753-4.
- [58] Dotan A, Dodiuk H, Laforte C, Kenig S. The relationship between water wetting and ice adhesion. J Adhes Sci Technol. 2009;23:1907-15. doi: 10.1163/016942409X12510925843078.
- [59] Petrenko VF, Peng S. Reduction of ice adhesion to metal by using self-assembling monolayers (SAMs). Can J Phys. 2003;81:387-93. doi: 10.1139/p03-014.
- [60] Bharathidasan T, Kumar SV, Bobji MS, Chakradhar RPS, Basu BJ. Effect of wettability and surface roughness on ice-adhesion strength of hydrophilic, hydrophobic and superhydrophobic surfaces. Appl Surf Sci. 2014;314:241–50. doi: 10.1016/j.apsusc. 2014.06.101.
- Kulinich SA, Farzaneh M. How wetting hysteresis influences ice [61] adhesion strength on superhydrophobic surfaces. Langmuir. 2009;25:8854-6. doi: 10.1021/la901439c.
- Yeong YH, Milionis A, Loth E, Sokhey J, Lambourne A. Atmospheric ice adhesion on water-repellent coatings: wetting and surface topology effects. Langmuir. 2015;31:13107-16. doi: 10.1021/acs. langmuir.5b02725.
- [63] Chen J, Liu J, He M, Li K, Cui D, Zhang Q, et al. Superhydrophobic surfaces cannot reduce ice adhesion. Appl Phys Lett. 2012;101:111603. doi: 10.1063/1.4752436.
- Banik A, Zhang C, Panyathong D, Tan KT. Effect of equienergetic [64] low-velocity impact on CFRP with surface ice in low temperature arctic conditions. Compos Pt B-Eng. 2022;236:109850. doi: 10.1016/j.compositesb.2022.109850.
- [65] Sarshar MA, Song D, Swarctz C, Lee J, Choi CH. Anti-icing or deicing: Icephobicities of superhydrophobic surfaces with hierarchical structures. Langmuir. 2018;34:13821-7. doi: 10.1021/acs. langmuir.8b02231.
- [66] Sun J, Wang C, Song J, Huang L, Sun Y, Liu Z, et al. Multi-functional application of oil-infused slippery Al surface: from anti-icing to

- corrosion resistance. J Mater Sci. 2018;53:16099-109. doi: 10.1007/ s10853-018-2760-z.
- [67] Song J, Huang W, Liu J, Huang L, Lu Y. Electrochemical machining of superhydrophobic surfaces on mold steel substrates. Surf Coat Technol. 2018;344:499-506. doi: 10.1016/j.surfcoat.2018.03.061.
- [68] Jin M, Shen Y, Luo X, Tao J, Xie Y, Chen H, et al. A combination structure of microblock and nanohair fabricated by chemical etching for excellent water repellency and icephobicity. Appl Surf Sci. 2018;455:883-90. doi: 10.1016/j.apsusc.2018.06.043.
- [69] Xu W, Song J, Sun J, Lu Y, Yu Z. Rapid fabrication of large-area, corrosion-resistant superhydrophobic Mg alloy surfaces. ACS Appl Mater Interfaces. 2011;3:4404-14. doi: 10.1021/am2010527.
- [70] Zhang J, Xu H, Guo J, Zhang Y, Chen T. A Superhydrophobic Self-Cleaning and Anti-Icing Aluminum Sheet Fabricated by Alkaline Solution, Adv Eng. Mater. 2021;23:2100347. doi: 10.1002/adem.202100347.
- [71] Lu Z, Wang P, Zhang D. Super-hydrophobic film fabricated on aluminium surface as a barrier to atmospheric corrosion in a marine environment. Corrosion Sci. 2015;91:287-96. doi: 10.1016/ i.corsci.2014.11.029.
- [72] Barthwal S, Lee B, Lim SH. Fabrication of robust and durable slippery anti-icing coating on textured superhydrophobic aluminum surfaces with infused silicone oil. Appl Surf Sci. 2019;496:143677. doi: 10.1016/j.apsusc.2019.143677.
- [73] Li X, Yin S, Huang S, Luo H, Tang Q. Fabrication of durable superhydrophobic Mg alloy surface with water-repellent, temperature-resistant, and self-cleaning properties. Vacuum. 2020;173:109172. doi: 10.1016/j.vacuum.2020.109172.
- [74] Xu W, Yi P, Gao J, Deng Y, Peng L, Lai X. Large-area stable superhydrophobic poly (dimethylsiloxane) films fabricated by thermal curing via a chemically etched template. ACS Appl Mater Interfaces. 2019;12:3042-50. doi: 10.1021/acsami.9b19677.
- [75] Wenxuan Y, Yuan Y, Guoyong L, Bing Z, Rongkai Y. The anti-icing/ frosting aluminum surface with hydrangea-like micro/nano structure prepared by chemical etching. Mater Lett. 2018;226:4-7. doi: 10.1016/j.matlet.2018.04.100.
- [76] Yang GF, Zhang H, Li HW, Lu MK, Zhai W, Cui J. Experimental study on the ice suppression characteristics of TC4 microstructure surface induced by femtosecond pulsed laser. Surf Coat Technol. 2020;405:126558. doi: 10.1016/j.surfcoat.2020.126558.
- [77] Liu M, Zhou R, Chen Z, Yan H, Cui J, Liu W, et al. Tunable hierarchical nanostructures on micro-conical arrays of laser textured TC4 substrate by hydrothermal treatment for enhanced anti-icing property. Coatings. 2020;10:450. doi: 10.3390/coatings10050450.
- [78] Milles S, Vercillo V, Alamri S, Aguilar-Morales AI, Kunze T, Bonaccurso E, et al. Icephobic performance of multi-scale lasertextured aluminum surfaces for aeronautic applications. Nanomaterials. 2021;11(1):135. doi: 10.3390/nano11010135.
- [79] Gaddam A, Sharma H, Karkantonis T, Dimov S. Anti-icing properties of femtosecond laser-induced nano and multiscale topographies. Appl Surf Sci. 2021;552:149443. doi: 10.1016/j.apsusc.
- [80] Hou W, Shen Y, Tao J, Xu Y, Jiang J, Chen H, et al. Anti-icing performance of the superhydrophobic surface with micro-cubic array structures fabricated by plasma etching. Colloid Surf A-Physicochem Eng Asp. 2020;586:124180. doi: 10.1016/j.colsurfa. 2019.124180.
- [81] Huang L, Song J, Lu Y, Chen F, Liu X, Jin Z, et al. Superoleophobic surfaces on stainless steel substrates obtained by chemical bath deposition. Micro Nano lett. 2017;12:76-81. doi: 10.1049/mnl. 2016.0576.

- Jia J, Fan J, Xu B, Dong H. Microstructure and properties of the super-hydrophobic films fabricated on magnesium alloys. J Alloy Compd. 2013;554:142-6. doi: 10.1016/j.jallcom.2012.11.117.
- [83] Zhu J, Zhang L, Dai X, Zhou B. One-step fabrication of a superhydrophobic copper surface by nano-silver deposition. AIP adv. 2020;10:075111. doi: 10.1063/5.0012620.
- Xiang T, Chen D, Lv Z, Yang Z, Yang L, Li C. Robust superhydrophobic coating with superior corrosion resistance. I Alloy Compd. 2019;798:320-5. doi: 10.1016/j.jallcom.2019.05.187.
- Tan J, Hao J, An Z, Liu C. Simple fabrication of superhydrophobic nickel surface on steel substrate via electrodeposition. Int J Electrochem Sci. 2017;12:40-9. doi: 10.20964/2017.01.15.
- Liu Y, Xue J, Luo D, Wang H, Gong X, Han Z, et al. One-step fabrication of biomimetic superhydrophobic surface by electrodeposition on magnesium alloy and its corrosion inhibition. J Colloid Interface Sci. 2017;91:313-20. doi: 10.1016/j.jcis.2016. 12.022.
- [87] Su F, Yao K. Facile fabrication of superhydrophobic surface with excellent mechanical abrasion and corrosion resistance on copper substrate by a novel method. Appl Mater Interfaces. 2014;6:8762-70. doi: 10.1021/am501539b.
- [88] Deng X, Mammen L, Butt HJ, Vollmer D. Candle soot as a template for a transparent robust superamphiphobic coating. Science. 2012;335:67-70. doi: 10.1126/science.1207115.
- [89] Liu L, Tang W, Ruan Q, Wu Z, Yang C, Cui S, et al. Robust and durable surperhydrophobic F-DLC coating for anti-icing in aircrafts engineering. Surf Coat Technol. 2020;404:126468. doi: 10.1016/j.surfcoat.2020.126468.
- [90] Niu W, Chen GY, Xu H, Liu X, Sun J. Highly transparent and selfhealable solar thermal anti-/deicing surfaces: when ultrathin MXene multilayers marry a solid slippery self-cleaning coating. Adv Mater. 2022;34:2108232. doi: 10.1002/adma.202108232.
- Lo TNH, Lee J, Hwang HS, Park I. Nanoscale coatings derived from fluoroalkyl and PDMS alkoxysilanes on rough aluminum surfaces for improved durability and anti-icing properties. ACS Appl Nano Mater. 2021;4:7493-7501. doi: 10.1021/acsanm.1c01526.
- [92] Peng C, Xing S, Yuan Z, Xiao J, Wang C, Zeng J. Preparation and anti-icing of superhydrophobic PVDF coating on a wind turbine blade. Appl Surf Sci. 2012;259:764-8. doi: 10.1016/j.apsusc.2012. 07.118.
- Tan X, Huang Z, Jiang L, Xiao T, Wang Y, Yang X, et al. A simple [93] fabrication of superhydrophobic PVDF/SiO2 coatings and their anti-icing properties. J Mater Res. 2021;36:637-45. doi: 10.1557/ s43578-020-00034-z.
- Yang Y, Shan L, Shen H, Qiu J. Manufacturing of robust superhydrophobic Wood surfaces based on PEG-functionalized SiO₂/ PVA/PAA/Fluoropolymer hybrid transparent coating. Prog Org Coat. 2021;154:106186. doi: 10.1016/j.porgcoat.2021.106186.
- [95] Cohen N, Dotan A, Dodiuk H, Kenig S. The thermo-mechanical mechanisms of reducing ice adhesion on superhydrophobic surfaces. Langmuir. 2016;32:9664-75. doi: 10.1021/acs.langmuir. 6b02495.
- Gwak Y, Park JI, Kim M, Kim HS, Kwon MJ, Oh SJ, et al. Creating [96] anti-icing surfaces via the direct immobilization of antifreeze proteins on aluminum. Sci Rep. 2015;5:1-9. doi: 10.1038/ srep12019.
- Zhang W, Xiang T, Liu F, Zhang M, Gan W, Zhai X, et al. Facile design and fabrication of superwetting surfaces with excellent wear-resistance. ACS Appl Mater Interfaces. 2017;9:15776-84. doi: 10.1021/acsami.7b02158.

- [98] Zeng Z, He J, Jie J, Zhou C, Chen B, Bao J, et al. Effect of perfluoropolyether and the micro nano structure of ZnO on anti-icing performance of fluorinated organic superhydrophobicity coatings on wind turbine blade surface. Mater Res Express. 2021;8:115008. doi: 10.1088/2053-1591/ac303d.
- Pan S, Guo R, Björnmalm M, Richardson JJ, Li L, Peng C, et al. Coatings super-repellent to ultralow surface tension liquids. Nat Mater. 2018:17:1040-7. doi: 10.1038/s41563-018-0178-2.
- Jiang G, Liu ZY, Hu JH. Superhydrophobic and photothermal PVDF/CNTs durable composite coatings for passive anti-icing/ active de-icing. Adv Mate Interfaces. 2021;9:2101704. doi: 10.1002/ admi.202101704.
- [101] Yin Z, Zhou D, Li M, Chen X, Xue M, Ou J, et al. A multifunction superhydrophobic surface with excellent mechanical/chemical/ physical robustness. Colloid Surf A-Physicochem Eng Asp. 2022;637:128258. doi: 10.1016/j.colsurfa.2022.128258.
- [102] Liu Y, Xu R, Luo N, Liu Y, Wu Y, Yu B, et al. All-day anti-icing/deicing coating by solar-thermal and electric-thermal effects. Adv Mater Technol. 2021;6:2100371. doi: 10.1002/admt.202100371.
- [103] Jiang G, Chen L, Zhang S, Huang H. Superhydrophobic SiC/CNTs coatings with photothermal deicing and passive anti-icing properties. ACS Appl Mater Interfaces. 2018;10:36505-11. doi: 10.1021/ acsami.8b11201.
- [104] Xie H, Wei J, Duan S, Zhu Q, Yang Y, Chen K, et al. Non-fluorinated and durable photothermal superhydrophobic coatings based on attapulgite nanorods for efficient anti-icing and deicing. Chem Eng J. 2022;428:132585. doi: 10.1016/j.cej.2021.132585.
- [105] Xue CH, Li HG, Guo XJ, Ding YR, Liu BY, An QF, et al. Superhydrophobic anti-icing coatings with self-deicing property using melanin nanoparticles from cuttlefish juice. Chem Eng J. 2021;424:130553. doi: 10.1016/j.cej.2021.130553.
- Li J, Jiao W, Wang Y, Yin Y, He X. Spraying pressure-tuning for the fabrication of the tunable adhesion superhydrophobic coatings between Lotus effect and Petal effect and their anti-icing performance. Chem Eng J. 2022;434:134710. doi: 10.1016/j.cej.2022.
- [107] Xie H, Zhao X, Li B, Zhang J, Wei J, Zhang J. Waterborne, nonfluorinated and durable anti-icing superhydrophobic coatings based on diatomaceous earth. New J Chem. 2021;45:10409-17. doi: 10.1039/D1NI01307F.
- [108] Zeng D, Li Y, Huan D, Liu H, Luo H, Cui Y, et al. Robust epoxymodified superhydrophobic coating for aircraft anti-icing systems. Colloid Surf A-Physicochem Eng Asp. 2021;628:127377. doi: 10.1016/j.colsurfa.2021.127377.
- [109] Zheng W, Teng L, Lai Y, Zhu T, Li S, Wu X, et al. Magnetic responsive and flexible composite superhydrophobic photothermal film for passive anti-icing/active deicing. Chem Eng J. 2022;427:130922. doi: 10.1016/j.cej.2021.130922.
- [110] Yin Y, Liu M, Wei W, Zhang Y, Gutowski V, Zhang W, et al. "Open-Mouth" mesoporous hollow micro/nano coatings based on POSS/ PDMS: fabrication, mechanisms, and anti-icing performance. Part Part Syst Charact. 2018;35:1800323. doi: 10.1002/ppsc.201800323.
- Shen Y, Wu Y, Tao J, Zhu C, Chen H, Wu Z, et al. Spraying fabri-[111] cation of durable and transparent coatings for anti-icing application: dynamic water repellency, icing delay, and ice adhesion. ACS Appl Mater Interfaces. 2018;11:3590-8. doi: 10.1021/acsami.
- [112] Zhou H, Chen R, Liu Q, Liu J, Yu J, Wang C, et al. Fabrication of ZnO/epoxy resin superhydrophobic coating on AZ31 magnesium alloy. Chem Eng J. 2019;368:262-72. doi: 10.1016/j.cej.2019.02.032.

- [113] Wu X, Zhao X, Ho JWC, Chen Z. Design and durability study of environmental-friendly room-temperature processable icephobic coatings. Chem Eng J. 2018;355:901–9. doi: 10.1016/j.cej.2018.07.204.
- [114] Brown S, Lengaigne J, Sharifi N, Pugh M, Moreau C, Dolatabadi A, et al. Durability of superhydrophobic duplex coating systems for aerospace applications. Surf Coat Technol. 2020;401:126249. doi: 10.1016/j.surfcoat.2020.126249.
- [115] Zhu T, Cheng Y, Huang J, Xiong J, Ge M, Mao J, et al. A transparent superhydrophobic coating with mechanochemical robustness for anti-icing, photocatalysis and self-cleaning. Chem Eng J. 2020;399:125746. doi: 10.1016/j.cej.2020.125746.
- [116] Chen H, Wang F, Fan H, Hong R, Li W. Construction of MOF-based superhydrophobic composite coating with excellent abrasion resistance and durability for self-cleaning, corrosion resistance, anti-icing, and loading-increasing research. Chem Eng J. 2021;408:127343. doi: 10.1016/j.cej.2020.127343.
- [117] Xie Q, Hao T, Zhang J, Wang C, Zhang R, Qi H. Anti-icing performance of a coating based on nano/microsilica particle-filled amino-terminated PDMS-modified epoxy. Coatings. 2019;9:771. doi: 10.3390/coatings9120771.
- [118] Ma T, Ma J, Yang C, Zhang J, Cheng J. Robust, multiresponsive, superhydrophobic, and oleophobic nanocomposites via a highly efficient multifluorination strategy. ACS Appl Mater Interfaces. 2021;13:28949–61. doi: 10.1021/acsami.1c07048.
- [119] Wang T, Zheng Y, Raji AR, Li Y, Sikkema WK, Tour JM. Passive antiicing and active deicing films. ACS Appl Mater Interfaces. 2016;8:14169–73. doi: 10.1021/acsami.6b03060.
- [120] Guo H, Liu M, Xie C, Zhu Y, Sui X, Wen C, et al. A sunlight-responsive and robust anti-icing/deicing coating based on the amphiphilic materials. Chem Eng J. 2020;402:126161. doi: 10.1016/j.cej.2020.126161.
- [121] Fenero M, Knez M, Saric I, Petravic M, Grande H, Palenzuela J. Omniphobic etched aluminum surfaces with anti-icing ability. Langmuir. 2020;36:10916–22. doi: 10.1021/acs.langmuir.0c01324.
- [122] Yu M, Liu M, Hou Y, Fu S, Zhang L, Li M, et al. Facile fabrication of biomimetic slippery lubricant-infused transparent and multifunctional omniphobic surfaces. J Mater Sci. 2020;55:4225–37. doi: 10.1007/s10853-019-04243-8.
- [123] Li H, Tang S, Zhou Q, Chen W, Yang X, Xing T, et al. Durable superhydrophobic cotton fabrics prepared by surface-initiated electrochemically mediated ATRP of polyhedral vinylsilsesquioxane and subsequent fluorination via thiol-Michael addition reaction. J Colloid Interface Sci. 2021;593:79–88. doi: 10.1016/j.jcis. 2021.03.006.
- [124] Zhang F, Xu D, Zhang D, Ma L, Wang J, Huang Y, et al. A durable and photothermal superhydrophobic coating with entwinned CNTs-SiO₂ hybrids for anti-icing applications. Chem Eng J. 2021;423:130238. doi: 10.1016/j.cej.2021.130238.
- [125] Gao J, Zhang Y, Wei W, Yin Y, Liu M, Guo H, et al. Liquid-infused micro-nanostructured MOF coatings (LIMNSMCs) with high antiicing performance. ACS Appl Mater Interfaces. 2019;11:47545–52. doi: 10.1021/acsami.9b16181.
- [126] Zhan X, Yan Y, Zhang Q, Chen F. A novel superhydrophobic hybrid nanocomposite material prepared by surface-initiated AGET ATRP and its anti-icing properties. J Mater Chem A. 2014;2:9390–9. doi: 10.1039/c4ta00634h.
- [127] Zhang Y, Guo H, Gao J, Wei W, Liu M, Zheng C, et al. Self-lubricated anti-icing MOF coating with long-term durability. Prog Org Coat. 2021;151:106089. doi: 10.1016/j.porgcoat.2020.106089.

- [128] Yin X, Zhang Y, Wang D, Liu Z, Liu Y, Pei X, et al. Integration of selflubrication and near-infrared photothermogenesis for excellent anti-icing/deicing performance. Adv Funct Mater. 2015;25:4237–45. doi: 10.1002/adfm.201501101.
- [129] Song J, Gao M, Zhao C, Lu Y, Huang L, Liu X, et al. Large-area fabrication of droplet pancake bouncing surface and control of bouncing state. ACS Nano. 2017;11:9259–67. doi: 10.1021/acsnano.7b04494.
- [130] Shao Y, Zhao J, Fan Y, Wan Z, Lu L, Zhang Z, et al. Shape memory superhydrophobic surface with switchable transition between "Lotus Effect" To "Rose Petal Effect". Chem Eng J. 2020;382:122989. doi: 10.1016/j.cej.2019.122989.
- [131] Yuan L, Wu T, Zhang W, Ling S, Xiang R, Gui X, et al. Engineering superlyophobic surfaces on curable materials based on facile and inexpensive microfabrication. J Mater Chem A. 2014;2:6952–9. doi: 10.1039/C4TA00672K.
- [132] Su C, Xu Y, Gong F, Wang F, Li C. The abrasion resistance of a superhydrophobic surface comprised of polyurethane elastomer. Soft Matter. 2010;6:6068–71. doi: 10.1039/C0SM00804D.
- [133] Wu X, Fu Q, Kumar D, Ho JWC, Kanhere P, Zhou H, et al. Mechanically robust superhydrophobic and superoleophobic coatings derived by sol-gel method. Mater Des. 2016;89:1302–9. doi: 10.1016/j.matdes.2015.10.053.
- [134] Ke C, Zhang C, Wu X, Jiang Y. Highly transparent and robust superhydrophobic coatings fabricated via a facile sol-gel process. Thin Solid Films. 2021;723:138583. doi: 10.1016/j.tsf.2021.138583.
- [135] Cai Y, Li J, Yi L, Yan X, Li J. Fabricating superhydrophobic and oleophobic surface with silica nanoparticles modified by silanes and environment-friendly fluorinated chemicals. Appl Surf Sci. 2018;450:102–11. doi: 10.1016/j.apsusc.2018.04.186.
- [136] Eshaghi A. Fabrication of transparent silica-silica nanotube/PFTS nano-composite thin films with superhydrophobic, oleophobic, self-cleaning and anti-icing properties. Opt Quantum Electron. 2020;52:1–13. doi: 10.1007/s11082-020-02656-3.
- [137] Zhou T, He Y, Wang T, Zhu Z, Xu R, Yu Q, et al. A review of the techniques for the mold manufacturing of micro/nanostructures for precision glass molding. Int J Extreme Manuf. 2021;3:042002. doi: 10.1088/2631-7990/ac1159.
- [138] Chen Y, Chen Y, Long J, Shi D, Chen X, Hou M, et al. Achieving a sub-10 nm nanopore array in silicon by metal-assisted chemical etching and machine learning. Int J Extreme Manuf. 2021;3:035104. doi: 10.1088/2631-7990/abff6a.
- [139] Zhang D, Liu R, Li Z. Irregular LIPSS produced on metals by single linearly polarized femtosecond laser. Int J Extreme Manuf. 2022;4:015301. doi: 10.1088/2631-7990/ac376c.
- [140] Wu B, Cui X, Jiang H, Wu N, Peng C, Hu Z, et al. A superhydrophobic coating harvesting mechanical robustness, passive antiicing and active de-icing performances. J Colloid Interface Sci. 2021;590:301–10. doi: 10.1016/j.jcis.2021.01.054.
- [141] Liao R, Li C, Yuan Y, Duan Y, Zhuang A. Anti-icing performance of ZnO/SiO₂/PTFE sandwich-nanostructure superhydrophobic film on glass prepared via RF magnetron sputtering. Mater Lett. 2017;206:109–12. doi: 10.1016/j.matlet.2017.06.127.
- [142] Zhu K, Li X, Su J, Li H, Zhao Y, Yuan X. Improvement of anti-icing properties of low surface energy coatings by introducing phase-change microcapsules. Polym Eng Sci. 2018;58:973–9. doi: 10.1002/pen.24654.
- [143] Goraj Z. An overview of the deicing and anti-icing technologies with prospects for the future. International Congress of the Aeronautical Sciences. Yokohama: Warsaw University of Technology; Vol. 29, 2004.